

Annual 30 m soybean yield mapping in Brazil using long-term satellite observations, climate data and machine learning

Xiao-Peng Song¹, Haijun Li¹, Peter Potapov², and Matthew C Hansen²

¹Texas Tech University

²University of Maryland

November 22, 2022

Abstract

Long-term spatially explicit information on crop yield is essential for understanding food security in a changing climate. Here we present a study that combines twenty-years of Landsat and MODIS data, climate and weather records, municipality-level crop yield statistics, random forests and linear regression models for mapping crop yield in a multi-temporal, multi-scale modeling framework. The study was conducted for soybean in Brazil, the world's largest producer and exporter of this commodity crop. Using a recently developed 30 m resolution, annual (2001-2019) soybean classification map product, we aggregated multi-temporal phenological metrics derived from Landsat and MODIS data over soybean pixels to the municipality scale. We combined phenological metrics with topographic features, long-term climate data, in-season weather data and soil variables as inputs to machine learning models. We trained a multi-year random forests model using yield statistics as reference and subsequently applied linear regression to adjust the biases in the direct output of the random forests model. This model combination achieved the best performance with a root-mean-square-error (RMSE) of 344 kg/ha (12% relative to long-term mean yield) and an r^2 of 0.69, on the basis of 20% withheld test data. The RMSE of the leave-one-year-out assessment ranged from 259 kg/ha to 816 kg/ha. To eliminate the artifacts caused by the coarse-resolution climate and weather data, we developed multiple models with different categories of input variables. Employing the per-pixel uncertainty estimates of different models, the final soybean yield maps were produced through per-pixel model composition. We applied the models trained on 2001-2019 data to 2020 data and produced a soybean yield map for 2020, demonstrating the predictive capability of trained machine learning models for operational yield mapping in future years. Our research showed that combining satellite, climate and weather data and machine learning could effectively map crop yield at high resolution, providing critical information to understand yield growth, anomaly and food security.

1 **Annual 30 m soybean yield mapping in Brazil using long-term satellite**
2 **observations, climate data and machine learning**

3
4 **Xiao-Peng Song^{1,*}, Haijun Li¹, Peter Potapov², Matthew C. Hansen²**

5 1. Department of Geosciences, Texas Tech University, Lubbock, TX, USA

6 2. Department of Geographical Sciences, University of Maryland, College Park, MD, USA

7 *Correspondence to: xiaopeng.song@ttu.edu

8
9 **Abstract**

10 Long-term spatially explicit information on crop yield is essential for understanding food security in a
11 changing climate. Here we present a study that combines twenty-years of Landsat and MODIS data,
12 climate and weather records, municipality-level crop yield statistics, random forests and linear regression
13 models for mapping crop yield in a multi-temporal, multi-scale modeling framework. The study was
14 conducted for soybean in Brazil, the world's largest producer and exporter of this commodity crop. Using
15 a recently developed 30 m resolution, annual (2001-2019) soybean classification map product, we
16 aggregated multi-temporal phenological metrics derived from Landsat and MODIS data over soybean
17 pixels to the municipality scale. We combined phenological metrics with topographic features, long-term
18 climate data, in-season weather data and soil variables as inputs to machine learning models. We trained a
19 multi-year random forests model using yield statistics as reference and subsequently applied linear
20 regression to adjust the biases in the direct output of the random forests model. This model combination
21 achieved the best performance with a root-mean-square-error (RMSE) of 344 kg/ha (12% relative to long-
22 term mean yield) and an r^2 of 0.69, on the basis of 20% withheld test data. The RMSE of the leave-one-

23 year-out assessment ranged from 259 kg/ha to 816 kg/ha. To eliminate the artifacts caused by the coarse-
24 resolution climate and weather data, we developed multiple models with different categories of input
25 variables. Employing the per-pixel uncertainty estimates of different models, the final soybean yield maps
26 were produced through per-pixel model composition. We applied the models trained on 2001-2019 data
27 to 2020 data and produced a soybean yield map for 2020, demonstrating the predictive capability of
28 trained machine learning models for operational yield mapping in future years. Our research showed that
29 combining satellite, climate and weather data and machine learning could effectively map crop yield at
30 high resolution, providing critical information to understand yield growth, anomaly and food security.

31 **Keywords**

32 Crop yield map; Random forests; Landsat; MODIS; Climate; Weather

33

34 **1. Introduction**

35 Reliable and timely information on crop production can inform commodity markets, insurance
36 companies, and policy interventions in response to natural disasters and human conflict (Benami et al.
37 2021; Li et al. 2022; Vroege et al. 2021). Estimating crop production over a spatial unit requires
38 information on crop harvested area and crop yield (i.e. production per unit area). Both harvested area and
39 yield can be derived from statistical field surveys or from satellite observations (Mulla 2013; Weiss et al.
40 2020) . While many methods exist in mapping crop type and estimating crop area using remote sensing
41 (e.g. Defourny et al. 2019; Gallego 2004; Gonzáles-Alonso and Cuevas 1993; Hu et al. 2021; King et al.
42 2017; Massey et al. 2017; Skakun et al. 2017; Song et al. 2017; Wardlow and Egbert 2008), studies are
43 increasingly investigating direct mapping of crop yield using remote sensing data. Crop yield maps can
44 facilitate a number of research or practical applications, such as climate impact evaluation and yield gap
45 analysis (Lobell 2013).

46 Mapping crop yield requires crop type masks as a prerequisite. When crop type masks are available, two
47 different strategies are commonly used to produce spatially explicit information on yield: the model-data
48 integration approach and the remote sensing-based empirical approach. The model-data integration
49 approach seeks to integrate crop simulation models with remote-sensing-derived biophysical variables for
50 yield forecasting (Delécolle et al. 1992; Moulin et al. 1998). Crop simulation models are developed using
51 comprehensive measurements recorded at the plot or field level, such as crop cultivar, sowing date, soil
52 property, water and nutrient inputs, weather, and plant physiological and morphological features (e.g. leaf
53 area index or LAI) (de Wit et al. 2019; Holzworth et al. 2014; Jones et al. 2003; Williams et al. 1989;
54 Yang et al. 2004). The modeled processes of crop growth can be used to predict crop productivity and to
55 evaluate the impacts of agricultural management and environmental stressors. Various techniques have
56 been proposed to “spatialize” crop process models using time-series of satellite-based soil, plant and
57 environmental variables, such as soil moisture, normalized difference vegetation index (NDVI), LAI,
58 green area index (GAI), and fraction of photosynthetically active radiation (fPAR) (Battude et al. 2016;

59 Claverie et al. 2012; de Wit et al. 2012; Doraiswamy et al. 2004; Duchemin et al. 2008; Huang et al.
60 2015; Ines et al. 2013; Kang and Özdoğan 2019; Nearing et al. 2012). Yet, a general limitation of
61 applying crop process models over large areas is the lack of sufficient and accurate information about
62 model inputs (Duchemin et al. 2008; Jin et al. 2018). Moreover, the model-data integration approach
63 usually does not serve the purpose of high-resolution yield mapping. The computational cost of per-pixel
64 crop simulation is high, but such barriers are being lifted by the recent development of cloud-computing
65 platforms such as Google Earth Engine (Gorelick et al. 2017).

66 The remote sensing-based empirical approach for crop yield mapping employs regression or machine
67 learning techniques to relate vegetation variables at key crop growth stages directly to yield. An early
68 work by Tucker et al. (1980) showed that time-integrated NDVI had significant correlation with grain
69 yield in a winter wheat field in Beltsville, Maryland. Becker-Reshef et al. (2010) demonstrated that
70 seasonal peak NDVI from the Moderate Resolution Imaging Spectroradiometer (MODIS) strongly
71 correlated with winter wheat yield in Kansas and Ukraine. Franch et al. (2015) extended the Becker-
72 Reshef et al. (2010) approach by including Growing Degree Day (GDD) information, which enabled yield
73 forecasting at about one month prior to peak NDVI. Funk and Budde (2009) found that time-integrated
74 MODIS NDVI adjusted to the onset of the rainy season correlated well with maize production in
75 Zimbabwe. Yield estimation may be improved by incorporating explicit phenology information using
76 other vegetation indices beyond NDVI. Building on the work of Funk and Budde (2009), Bolton and
77 Friedl (2013) suggested that MODIS-based two-band Enhanced Vegetation Index (EVI2) standardized by
78 the greenup date correlated better than NDVI with county-level yield for maize, but indifferent for
79 soybean, over central US. Similarly, Sakamoto et al. (2013) applied a phenology detection method to
80 identify corn silking stage and demonstrated that MODIS-derived Wide Dynamic Range Vegetation
81 Index (WDRVI) (Gitelson 2004) at that stage had high correlations with yield over major corn producing
82 states of the US. Johnson (2014) proved that daytime land surface temperature (LST) negatively
83 correlated with maize and soybean yield in the US while MODIS peak NDVI positively correlated with

84 yield. Recently, Skakun et al. (2021) investigated the utility of Landsat-8, Sentinel-2, WorldView-3 and
85 Planet data for corn and soybean yield mapping over a number of sample sites in Iowa, and found that
86 surface reflectance from red-edge bands performed better than vegetation indices to reveal field-level
87 yield variability. Lobell et al. (2015) developed an approach that used simulations from a crop model to
88 train a regression to predict yields from satellite observations, and the approach was tested in industrial as
89 well as smallholder systems (Jin et al. 2019).

90 While regression-based methods are straightforward to implement, more complex algorithms and data
91 analytic techniques such as machine learning algorithms are being increasingly investigated. Using NDVI
92 from the Advanced Very High Resolution Radiometer (AVHRR) and MODIS, Li et al. (2007) compared
93 multivariate linear regression and artificial neural networks for modeling corn and soy yield over a
94 number of sample counties in the US corn belt. Likewise, Johnson et al. (2016) compared the
95 performance of multiple linear regression and nonlinear Bayesian neural networks and model-based
96 recursive partitioning for forecasting barley, canola and spring wheat yields on the Canadian Prairies.
97 Based on the finding that NDVI and LST highly correlated with crop yield, Johnson (2014) built a
98 regression tree model using multiple years of county-level yield statistics as reference and applied the
99 model to MODIS data to forecast corn and soybean yield at 250 m resolution in the US. Cai et al. (2019)
100 tested the utility of the enhanced vegetation index (EVI) from MODIS and solar-induced chlorophyll
101 fluorescence from GOME-2 and SCIAMACHY, and regression and machine learning algorithms for
102 wheat yield prediction in Australia, and found that the combination of MODIS EVI, climate data and
103 support vector machines (SVM) could achieve high performance in yield prediction. Mateo-Sanchis et al.
104 (2019) proposed a multi-sensor metric, namely the time lag between MODIS EVI and vegetation optical
105 depth (VOD) from the Soil Moisture Active Passive (SMAP) satellite, as input to nonlinear kernel ridge
106 regression for modeling county-scale crop yield in the US corn belt. Deep learning algorithms are also
107 being explored in yield estimation. Schwalbert et al. (2020) developed a method for in-season soybean
108 yield forecasting using the Long-Short Term Memory (LSTM) algorithm, MODIS-based NDVI, EVI and

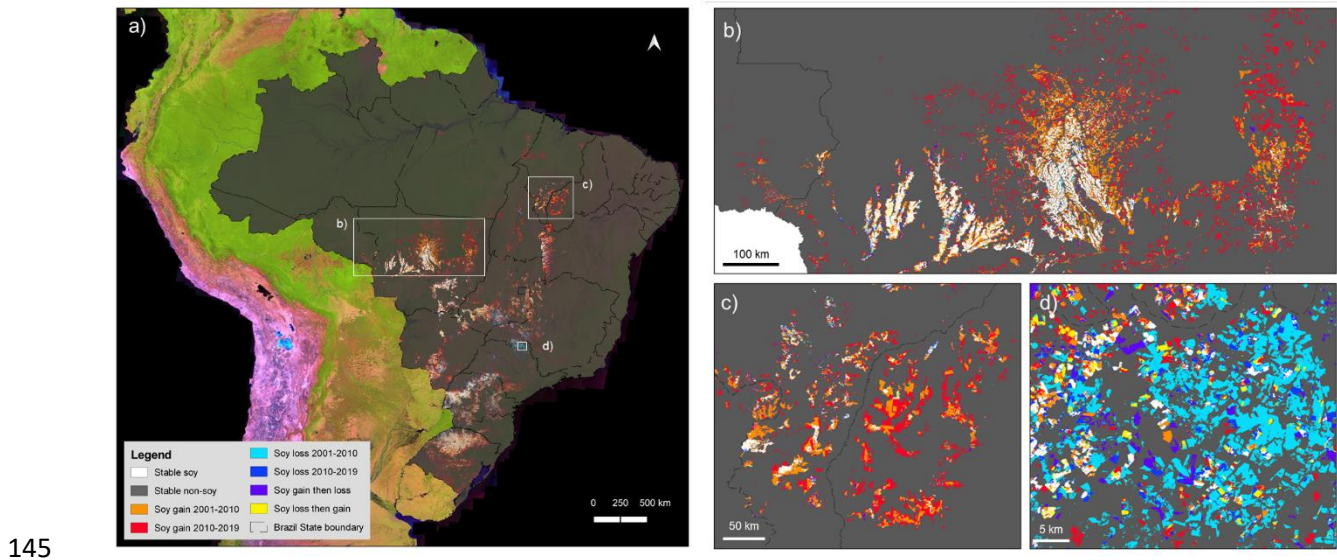
109 LST data, and precipitation data at the municipality scale in the Brazilian state of Rio Grande do Sul.
110 Recent research has also started to combine machine learning and crop models by incorporating output
111 variables from crop models as input features to machine learning algorithms for yield estimation (Paudel
112 et al. 2021; Shahhosseini et al. 2021).

113 These previous studies clearly show that crop yield estimation represents a continually active line of
114 research in remote sensing. The primary goal is to improve the accuracy of yield estimation using new
115 data and techniques, and/or to advance the date of in-season forecasting. However, most previous studies
116 are demonstrative research with limited spatial extents and/or temporal span in their study areas. Studies
117 exploring the long-term satellite data archives to evaluate the variability of crop yields also exist albeit
118 over small study areas (e.g. Gao et al. 2018; Liu et al. 2020). More importantly, common to most yield
119 mapping studies, crops in the temperate climate zone are often the target crops and target regions. Long-
120 term, large-area crop yield mapping in the tropics does not exist. Unlike the temperate region where
121 climate conditions are relatively homogenous and crop phenologies are largely synchronous, cropping
122 systems in the tropics are more complex in the sense that planting and harvesting schedules could be
123 substantially different for the same crop (e.g. soybean in Brazil) (Song et al. 2021). Statistics-based
124 phenological metrics derived from time-series of satellite data can capture the salient features of
125 vegetation phenology while maintaining high spatial and temporal data consistency, and thus, provide a
126 unique advantage to large-area vegetation type mapping (DeFries et al. 1995; Hansen et al. 2013; Song et
127 al. 2018). The main objective of this study is to explore the utility of statistical metrics derived from
128 Landsat and MODIS data as well as machine learning algorithms for high-resolution, long-term crop
129 yield mapping in the tropics. Producing long-term spatially explicit yield information is especially
130 imperative in tropical countries, where agricultural production is growing rapidly, causing detrimental
131 impacts to natural environment (Gibbs et al. 2010; Potapov et al. 2022; Song et al. 2018; Zalles et al.
132 2021). We focus on annual soybean yield in Brazil over 2001-2020 in this study.

133 **2. Data and Methods**

134 **2.1. Study area**

135 Our study area covers the southern hemisphere portion of Brazil. Brazil is the world's leading producer
 136 and exporter of soybeans, accounting for more than 35% of global production and about half of the
 137 world's total export (FAO 2020). Based on statistics from the Food and Agriculture Organization of the
 138 United Nations (FAO), soybean production in Brazil has tripled from 37.9 million tons in 2001 to 114.3
 139 million tons in 2019 (FAO 2020). Over the same time period, soybean cultivation area in Brazil increased
 140 from 14.0 Mha to 35.9 Mha, and the national average yield increased from 2.71 to 3.18 tons/ha with the
 141 maximum yield of 3.39 tons/ha achieved in 2018 (FAO 2020). The dramatic increase in soybean
 142 cultivation in Brazil (Figure 1) has directly and indirectly caused widespread natural vegetation loss and
 143 cascading environmental impacts in the Amazon, Cerrado and other biomes (Song et al. 2021a; Zalles et
 144 al. 2019).



146 **Figure 1.** Soybean expansion in Brazil mapped using satellite data. (a) Soybean change during 2001-2010
 147 and 2010-2019. For simplicity to visualize, the annual 2001-2019 classification maps are used to create
 148 bi-temporal change layers. Landsat mosaic of South America is used as the backdrop in (a), and gray
 149 shaded area represents the study area of Brazil. Regional details over two soybean expansion frontiers are

150 shown in (b) Mato Grosso and (c) MaToPiBa (Maranhao, Tocantins, Piaui and Bahia). Reduction in
151 soybean cultivation was observed along the border between Sao Paulo and Minas Gerais, shown in (d).

152

153 **2.2. Satellite data and products**

154 We used Landsat and MODIS as the main satellite data to derive vegetation characteristics of soybean
155 plants, as they represent the most consistent satellite data records over the past two decades. According to
156 the United States Department of Agriculture (USDA) crop calendars for Brazil, soybeans in Brazil are
157 typically planted in October to December and harvested in March to May
158 (https://ipad.fas.usda.gov/rssiws/al/crop_calendar/br.aspx). In our study, all Landsat and MODIS
159 observations acquired between November 1st and April 30th of the next year from 2000 to 2019 were
160 processed. The MODIS surface reflectance (SR) data in blue (469 nm), green (555 nm), red (645 nm),
161 near-infrared (NIR, 858 nm), shortwave infrared (SWIR, 1640 nm and 2130 nm) and thermal (11,030 nm)
162 wavelengths were obtained as 16-day composites from the MOD44C product, same as the MOD09GA,
163 MOD09GQ and MODTBGA v006 products (Vermote and Wolfe 2015). Landsat images acquired by the
164 Thematic Mapper (TM), Enhanced Thematic Mapper Plus (ETM+), and Operational Land Imager (OLI),
165 with blue, green, red, NIR, and SWIR bands, were converted from top-of-atmosphere reflectance to
166 normalized surface reflectance (NSR) through an automated data processing system (Potapov et al. 2020).
167 Using MODIS SR as normalization target, the system corrected atmospheric and anisotropic effects of
168 Landsat after at-sensor radiance calculation, cloud, shadow and haze masking. The Landsat NSR, from all
169 sensors, was then processed to 16-day composites consistent with the MODIS product. Both Landsat
170 NSR and MODIS SR 16-day time-series were used to create seasonal phenological metrics, including
171 NDVI, EVI, normalized difference water index (NDWI) and other band ratio indices (Table 1). A
172 complete description of Landsat data processing and the freely available software tools to generate
173 phenological metrics is provided in Potapov et al. (2020).

174 **Table 1.** Input features for modeling and mapping soybean yield in Brazil. Please see Supplementary
 175 Information for the complete list of variables.

Category	Input Features	N
Landsat-based	Seasonal vegetation phenological metrics derived from Blue, Green, Red, NIR, SWIR1, SWIR2 and thermal bands	50
MODIS-based	Seasonal vegetation phenological metrics derived from Blue, Green, Red, NIR, SWIR1, SWIR2 and thermal bands	24
Topographic	DEM and Slope	2
Climate	Long-term (1971-2000 average) climate data, monthly (October to May) TMP (mean 2 m temperature), DTR (diurnal 2 m temperature range), PRE (precipitation rate), VAP (vapor pressure), WET (wet days), CLD (cloud cover), TMN (minimum 2 m temperature), TMX (maximum 2 m temperature) and PET (potential evapotranspiration)	72
Weather	Annual (2000 through 2019) in-season weather data, monthly (October to May) TMP, DTR, PRE, VAP, WET, CLD, TMN, TMX and PET	72
Soil	Water storage capacity, topsoil and subsoil bulk density, cation exchange capacity of the clay fraction in the topsoil and subsoil, topsoil and subsoil clay, sand and silt fractions, topsoil and subsoil pH, and area weighted topsoil and subsoil carbon content	15

176

177 We used a recently developed 30 m resolution ($0.00025^\circ \times 0.00025^\circ$), annual, 2001-2019 soybean
 178 classification map product (Song et al. 2021a) as masks to constrain the yield modeling and mapping to
 179 identified soybean pixels (Figure 1). For simplicity and consistent with the soybean classification map
 180 product, in this study we refer to a cropping year by the harvest year. For example, year 2001 indicates
 181 the 2000/01 cropping year. The soybean classification product was developed using the above Landsat
 182 and MODIS data as input in addition to 30 m resolution topographic features from the Shuttle Radar
 183 Topography Mission (SRTM) data. Continentally distributed field observations collected over three years
 184 (2017, 2018 and 2019) were used as training to calibrate a multi-year bagged decision tree model for

185 soybean classification. The overall accuracy of the soybean classification maps for the years of 2017,
186 2018, and 2019, where we had probability field sample for validation, was 96%, 94% and 96%,
187 respectively, with high and balanced producer's and user's accuracies (Song et al. 2021a).

188 **2.3. Climate and weather data**

189 Monthly climate and weather covariates were obtained from the Climatic Research Unit gridded Time
190 Series (CRU TS) version 4.04 dataset (Harris et al. 2020). The variables included TMP (mean 2 m
191 temperature), DTR (diurnal 2 m temperature range), PRE (precipitation rate), VAP (vapor pressure),
192 WET (wet days), CLD (cloud cover), TMN (minimum 2 m temperature), TMX (maximum 2 m
193 temperature) and PET (potential evapotranspiration) at a spatial resolution of $0.5^\circ \times 0.5^\circ$. We calculated
194 monthly average values from 1971 to 2000 for the months from October to May to represent long-term
195 climatology. For each year between 2000 to 2019, we directly used the monthly values for the months
196 from October to May to represent in-season weather (Table 1).

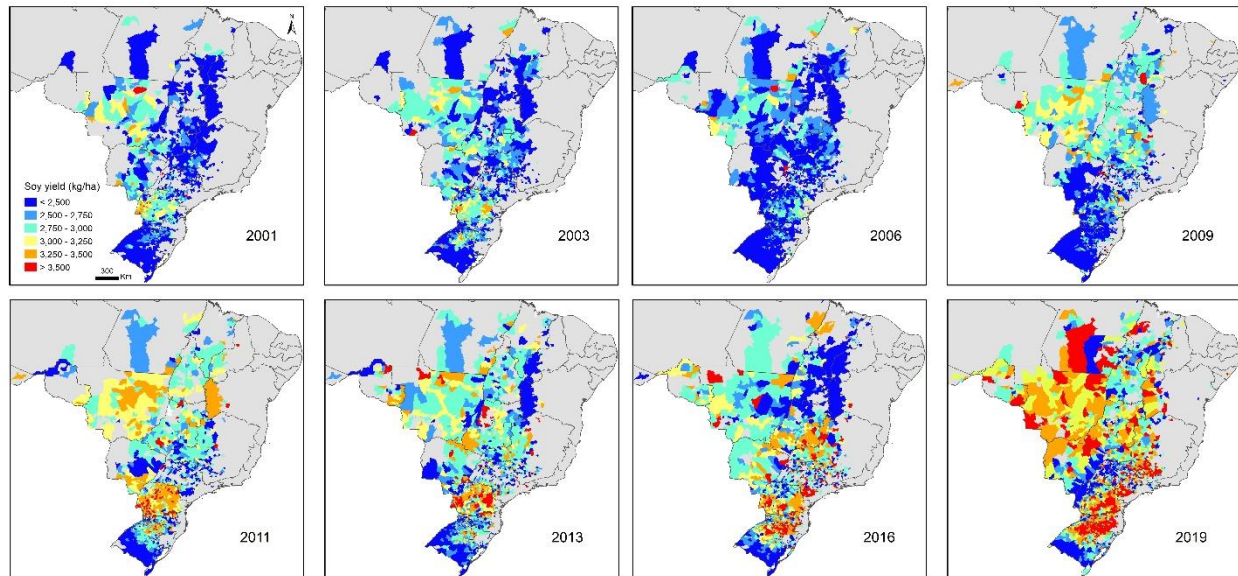
197 **2.4. Soil data**

198 The RegridDED Harmonized World Soil Database v1.2 at $0.05^\circ \times 0.05^\circ$ spatial resolution
199 (FAO/IIASA/ISRIC/ISSCAS/JRC 2012; Wieder et al. 2014) were obtained and processed similar to the
200 climate and weather data. The soil variables included available water storage capacity, topsoil (0-30 cm)
201 and subsoil (30-100 cm) bulk density, cation exchange capacity of the clay fraction in the topsoil and
202 subsoil, topsoil and subsoil clay, sand and silt fractions, topsoil and subsoil pH, and area weighted topsoil
203 and subsoil carbon content (Table 1).

204 **2.5. Municipal yield statistics**

205 We obtained soybean yield statistics at the municipality scale for every year between 2001 and 2019 from
206 the Brazilian Institute of Geography and Statistics (IBGE) Municipal Agricultural Production database
207 (<https://sidra.ibge.gov.br/>). The size of the municipalities where soybeans are cultivated varies widely
208 from south (small) to north (large), with a median size of approximately 48 Kha, the first quantile of 22

209 Kha and the third quantile of 135 Kha. These yield statistics were used as reference data for training and
 210 evaluation (Figure 2).

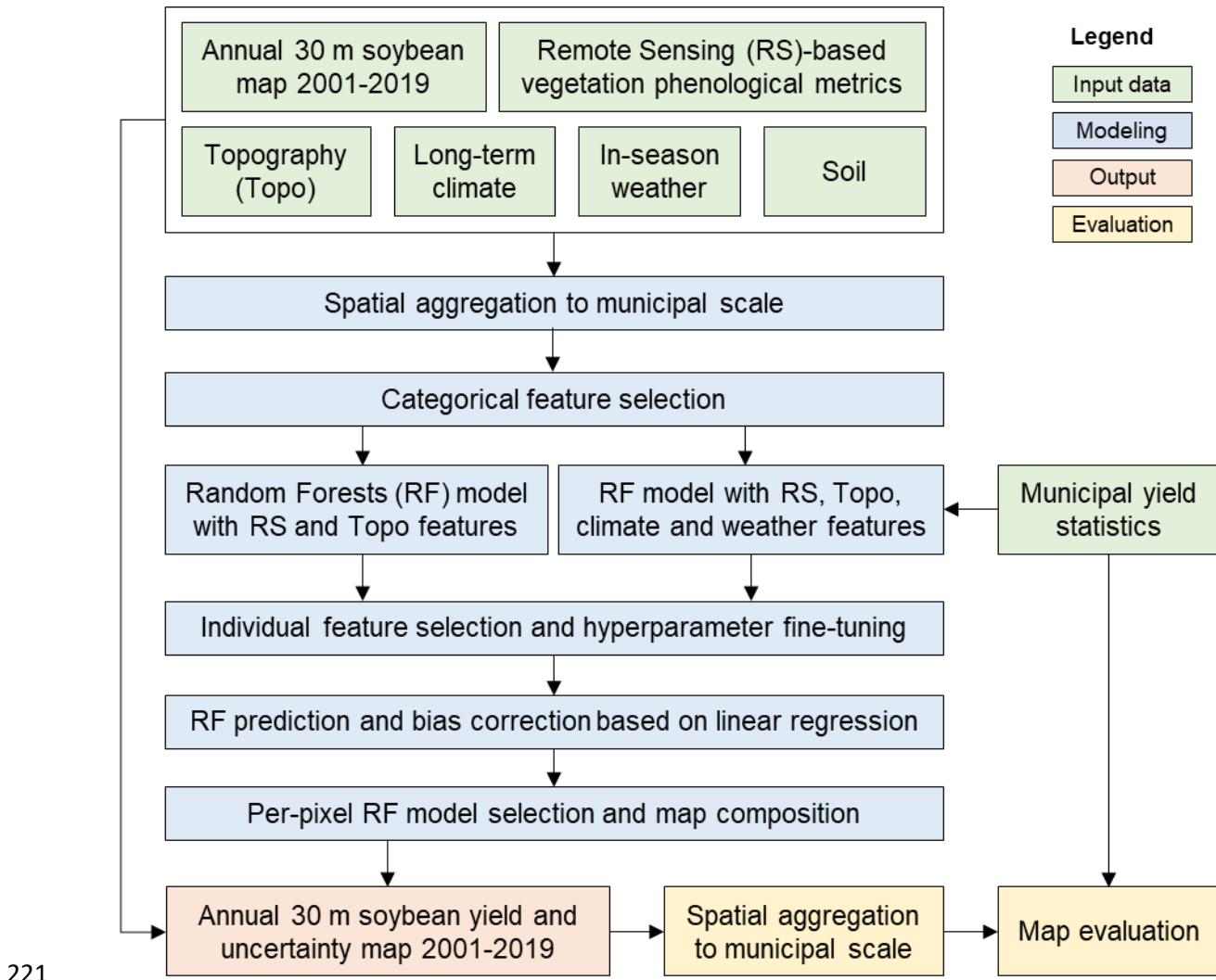


211
 212 **Figure 2.** Municipality-level yield statistics from the Brazilian Institute of Geography and Statistics
 213 (IBGE) were used as reference for modeling and mapping soy yield.

214

215 2.6. Modeling yield

216 The overall workflow of modeling and mapping soybean yield is presented in Figure 3. Major steps
 217 include spatial aggregation of remote sensing (RS)-based vegetation phenological metrics, topographic
 218 (topo) features, climate, weather, and soil variables to municipal scale, categorical feature selection,
 219 random forests (RF) (Breiman 2001) model training, RF prediction, bias correction, per-pixel RF model
 220 selection and composition, and map evaluation. Details of each step are described as follows.



221

222 **Figure 3.** Overall workflow of mapping annual soybean yield 2001-2019 using satellite data, climate,
 223 weather, soil and topography data, municipality statistics, random forests and linear regression models.
 224 Two random forests models were trained and implemented with more details reported in the text.

225

226 The $0.5^\circ \times 0.5^\circ$ climate and weather data, and the $0.05^\circ \times 0.05^\circ$ soil data were first resampled using
 227 nearest resampling to $0.00025^\circ \times 0.00025^\circ$ to match the spatial resolution of the soybean classification
 228 map, remote sensing data and topographic features. With the annual soybean classification map as a
 229 mask, we aggregated these input datasets to municipal scale by taking the average value over soybean
 230 pixels in each municipality. The spatial aggregation step was conducted for every year independently

231 between 2001 and 2019. To remove the non-soybean and low-soybean municipalities, we selected the
232 municipalities with annual soybean pixels $\geq 50,000$, resulting in a total of 15,784 municipalities across the
233 19-year period. These municipalities contained 95% of all mapped soybean pixels over the study period.

234 To investigate the relative utilities of these multi-source, multi-resolution input datasets for yield
235 modeling, we conducted three progressive experiments using categorical feature selection. Specifically,
236 we built three random forests models with (1) RS and topo features as input, (2) RS, topo, climate and
237 weather features as input, and (3) RS, topo, climate, weather and soil features as input. Performance of
238 model #1 represents the utility of RS and topo features to model yield. Improved performance of model
239 #2 over model #1 would represent the value of weather and climate data. Likewise, improved
240 performance of model #3 over model #2 would represent the value of the soil variables.

241 Municipal yield statistics were used as reference for all three models. For each model, we randomly
242 selected 80% municipalities as training ($n = 12,649$) and the remaining 20% was reserved for independent
243 test ($n = 3,135$), with both training and test data covering all 19 years. We calculated root-mean-square-
244 error (RMSE), mean bias error (MBE), mean absolute error (MAE), and r^2 using both training and test
245 data for all three models. To further enhance the robustness of the model evaluation and to eliminate
246 potential bias from a particular realization of sampling, we implemented a Monte Carlo method and
247 repeated the random training/test split, model training and evaluation 100 times. The final model
248 performance was represented using box plots of RMSE, MBE, MAE and r^2 of the 100 runs.

249 In addition to model evaluation with 20% withheld test data, we also conducted the leave-one-year-out
250 model assessment. For every year between 2001 and 2019, we used 18-years of data to calibrate the
251 random forests models and used the model to predict over the left-out year. For the left-out year, we
252 compared the predicted yield with reference statistics and calculated error metrics.

253 Our model assessment revealed that climate and weather variables significantly improved model
254 performance, but soil variables did not further improve model performance (more details are provided in

255 the Results and Discussion sections). Therefore, the model with RS, topo, climate and weather variables
256 as input (i.e. model #2) was selected as the primary model for yield estimation. However, due to the
257 coarse spatial resolution ($0.5^\circ \times 0.5^\circ$) of the climate and weather data, spatial grid patterns were noticed in
258 some regions. To remove these artifacts, we implemented model #1 (RS and topo features as input) as a
259 secondary model, and results of the two models were combined (see more details below).

260 To improve computational efficiency, we conducted individual feature selection for both models. For
261 each RF model, we trained the model using all features as input, ranked each feature and selected the top
262 features with a cumulative importance of greater than 95%. We also constructed a correlation matrix of
263 the features and removed those less important features that had a correlation coefficient of greater than
264 0.95 with the more important ones. Error metrics were calculated for all as well as selected features to
265 demonstrate the comparable performance of trained models. We implemented the random forest classifier
266 function in the sklearn package in python. The RF parameters fine-tuned included n_estimators (number
267 of trees), max_features (number of features to consider at every split), max_depth (maximum number of
268 levels in a tree), min_samples_split (minimum number of samples required to split a node),
269 min_samples_leaf (minimum number of samples required at each leaf node). We applied a randomized
270 search on hyper-parameters followed by a grid search to determine the exact values for these parameters.

271 The immediate output of the two RF models include predicted soybean yield, represented as the mean
272 value of all trees in the forest, and associated uncertainty, represented as the standard deviation of all trees
273 in the forest. For continuous variables, random forests could generate underestimation at the high-end of
274 the variable and overestimation at the low-end of the variable because of the effect of “regression to the
275 mean” (Huang et al. 2016; Zhang and Lu 2012). Such is the case for our yield modeling in this study. To
276 correct these systematic biases, we followed Zhang and Lu (2012) and Huang et al. (2016), and applied
277 linear regression using the municipal yield statistics as the dependent variable and the RF-predicted yield
278 as the independent variable. The derived linear equation was subsequently applied to the adjust the RF-
279 predicted yield and uncertainty.

280 We implemented the two calibrated random forest models (models #1 and #2) and their associated linear
281 regressions independently using the annual input datasets. The outputs were two sets of 30 m resolution
282 soybean yield and uncertainty maps for every year between 2001 and 2019. We created a final soybean
283 yield and uncertainty map for every year through per-pixel composition, where, for every pixel, the
284 soybean yield and associated uncertainty were selected from the model with a smaller uncertainty.

285 **2.7. Yield map evaluation**

286 We evaluated the quality of the annual, 30 m resolution soybean yield maps at the municipal scale.
287 Average yield was derived from the maps, and compared to municipal yield statistics as reference. We
288 computed the difference of the two datasets and constructed a histogram. We calculated RMSE, MAE,
289 MBE, and r^2 , and created scatter plots using the 19 years of data. We also calculated these error metrics
290 for every year to evaluate the temporal consistency of the yield map time series.

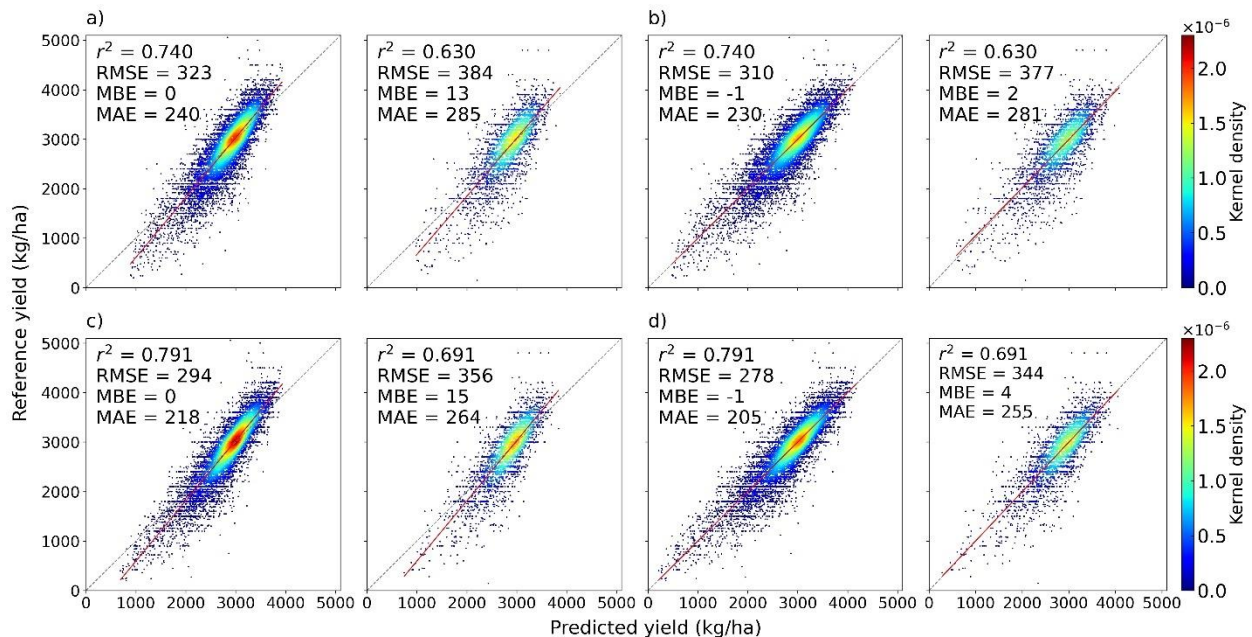
291 **3. Results**

292 **3.1. Model selection and performance**

293 Using remote sensing-based vegetation phenological metrics and topographic features as input to random
294 forests (model #1) produced an r^2 of 0.74, an RMSE of 323 kg/ha, an MBE of 0 kg/ha and a MAE of 240
295 kg/ha for training data. Compared to the 2001-2019 national average yield of 2,869 kg/ha, this RMSE
296 represents 11% error. Adding climate and weather variables to input (model #2) significantly improved
297 model performance, as represented by the increase in r^2 and reduction in RMSE and MAE, for both
298 training and test data. The improved model had an r^2 of 0.79, an RMSE of 294 kg/ha, an MBE of 0 kg/ha
299 and a MAE of 218 kg/ha for training data, and an r^2 of 0.69, an RMSE of 356 kg/ha, an MBE of 15 kg/ha
300 and a MAE of 264 kg/ha for test data. Adding soil variables to input (model #3) showed little to no value
301 in further improving model performance. Therefore, we discarded model #3 and implemented model #1
302 and #2 in this study. Both model #1 and #2 were chosen because although climate and weather data
303 demonstrated considerable utility in modeling soybean yield, their coarse spatial resolution ($0.5^\circ \times 0.5^\circ$)

304 caused apparent grid patterns when the model was applied to 30 meter spatial resolution, whereas model
 305 #1 generated spatially coherent results. Moreover, individual feature selection not only improved
 306 computational efficiency but also improved model accuracy. Consistent for all model categories, there
 307 remained some differences between training and test, indicating potential overfitting of the models. This
 308 was likely due to the lack of high-quality soil data and other important agricultural management variables
 309 (e.g. fertilizer use) in the model (please see more details in the Discussion section).

310 Predicted yield from random forests models were highly consistent with reference yield from municipal
 311 statistics (Figure 4). However, the direct outputs of the random forests models under-estimated yield at
 312 the high end and over-estimated yield at the low end (Figure 4a and 4c). Applying a linear regression
 313 successfully corrected these systematic biases for both models (Figure 4b and 4d). Moreover, the overall
 314 model performance was also slightly improved, as demonstrated by the reduction in RMSE and MAE for
 315 both training and test results. For instance, the training accuracy in terms of RMSE was reduced from 294
 316 to 278 kg/ha and the test accuracy was improved from 356 to 344 kg/ha for model #2 after bias
 317 adjustment (Figure 4a vs 4b).



318

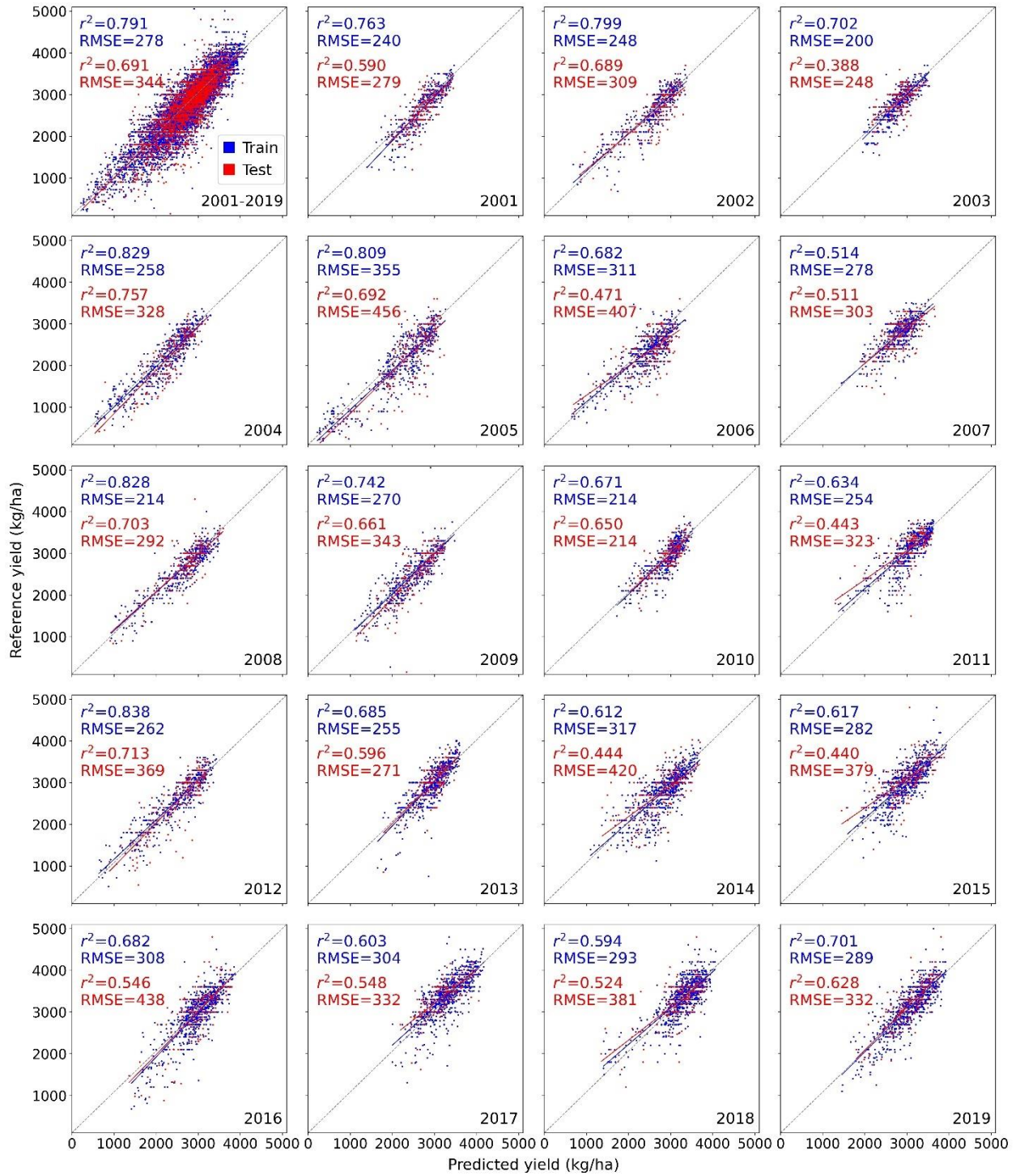
319 **Figure 4.** Performance of yield models before and after systematic bias adjustment using linear
320 regression. a) Random forests (RF)-predicted soybean yield against reference yield from municipal
321 statistics. Input data for RF include remote sensing, topographic features, climate and weather variables.
322 The left panel is density scatter plots using training data and the right panel is density scatter plots of
323 independent test data. The red lines on both panels represent the linear regression line. b) Same as a), but
324 a linear regression was applied to adjust bias in RF outputs. c) RF-predicted soybean yield against
325 reference yield. Input data for RF only include remote sensing and topographic features. d) Same as c),
326 but after linear bias adjustment.

327

328 Although the model was trained using all 19-years of data as input, evaluation of model performance at
329 the annual time scale revealed consistent model performance across all 19 years (Figure 5). Based on the
330 withheld test data, the 19-year overall RMSE was 344 kg/ha and the r^2 was 0.69. The RMSE represents
331 12% error relative to long-term yield mean. The annual RMSE values ranged from 214 kg/ha in 2010 to
332 456 kg/ha in 2005, and the annual r^2 values ranged from 0.39 in 2003 to 0.76 in 2004. No significant
333 systematic bias was observed for any of the years (Figure 5).

334 The leave-one-year-out model assessment revealed that the yield models performed well for most of the
335 19 years, but performed relatively poorly for 2005 and 2015 with notably higher RMSE and lower r^2 ,
336 respectively (Figure 6). The RMSE of the leave-one-year-out assessment ranged from 259 kg/ha to 816
337 kg/ha. These results are in general comparable to regional studies of satellite-based soybean yield
338 mapping in the Midwest of the United States (Lobell et al. 2015) and Southern Brazil (Schwalbert et al.
339 2020). Both 2005 and 2015 did not show notable performance deficiency when data of the two years were
340 included in training (Figure 5). Comparison between annual accuracies of the two model assessments
341 (Figures 5 and 6) suggests that model trained with long time series of data generally perform well for
342 unseen years. The comparison also highlights the significance of including both good and poor harvesting
343 years in training for enhancing the temporal generalization and predictive capability of trained models.

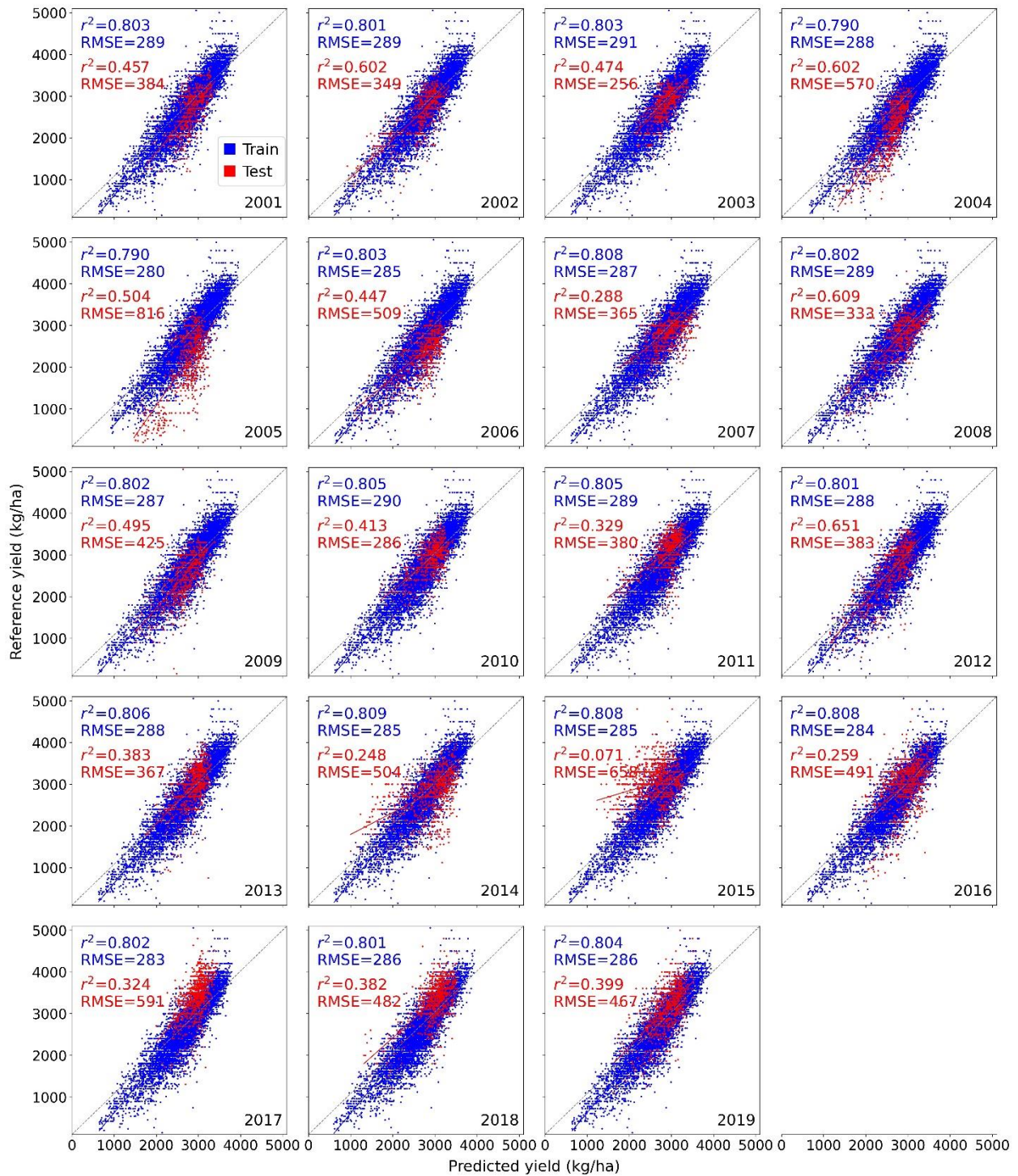
344



345

346 **Figure 5.** Performance of yield model at an annual time scale. X-axis represents model-predicted yield,
 347 and y-axis represents reference yield from municipal statistics. The top-left scatter plot is a combination
 348 of the two scatter plots in Figure 5b. Scatter plots are made using training data and withheld test data.
 349 Input data for model include remote sensing, topographic features, climate and weather variables.

350



351

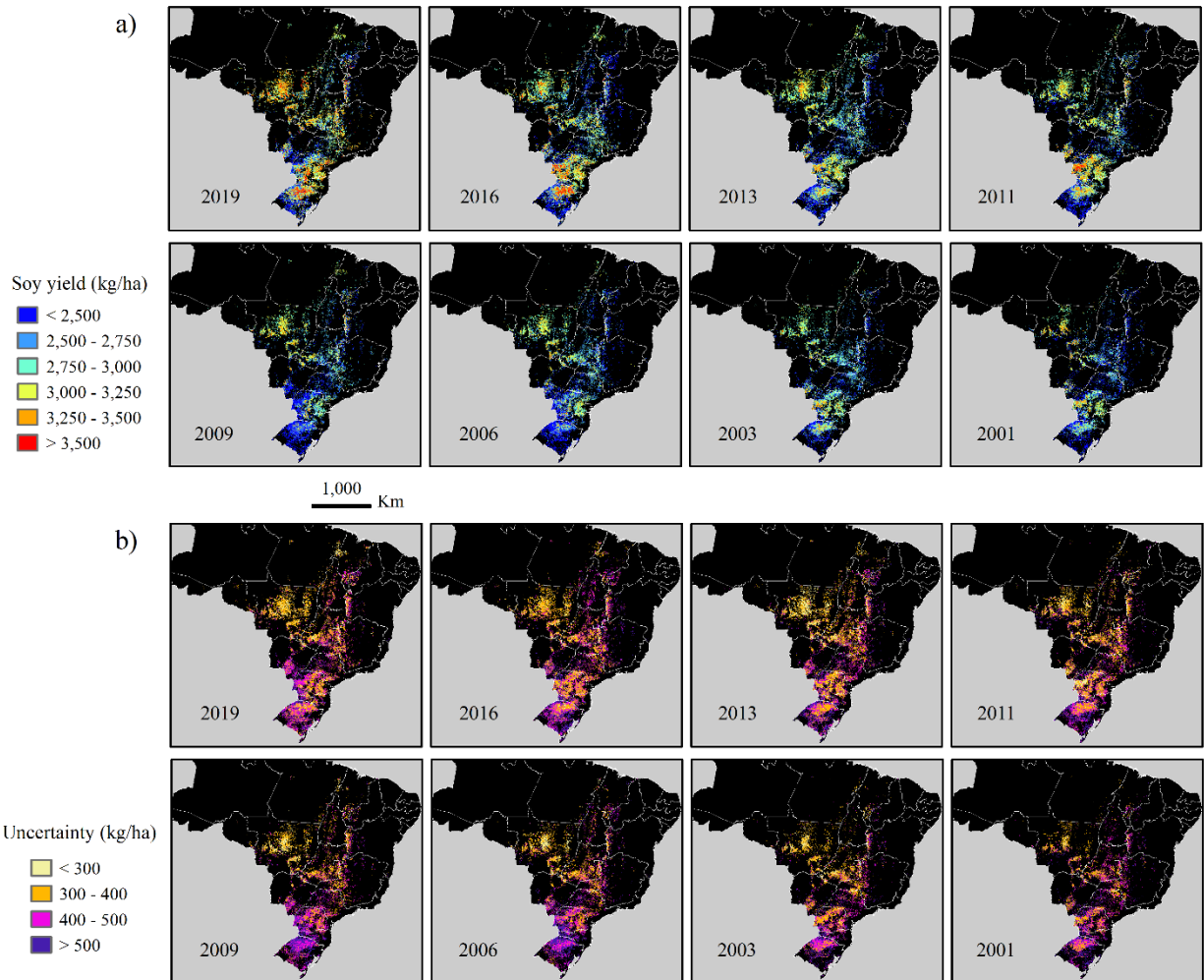
352 **Figure 6.** Leave-one-year-out model assessment. For each year between 2001 and 2019, 18-years of data
 353 were used to training the model (blue dots and text), which was used to predict over the left-out year.

354 Municipal statistics of the left-out year were used as reference to evaluate the model performance (red
355 dots and text).

356

357 **3.2. Annual soybean yield and uncertainty maps**

358 Implementing the calibrated random forests and linear regression models at 30 m spatial resolution
359 generated spatially and temporally coherent soybean yield distributions across Brazil from 2001 to 2019
360 (Figure 7a). Considerable spatial heterogeneity in soybean yields was observed across the country. In
361 2001, the highest soybean yield regions included central Mato Grosso and western Parana (also see Figure
362 2a), and the lowest yield regions included Rio Grande do Sul, eastern Goias, western Minas Gerais, and
363 western Bahia. Increase in soybean yield was found in many regions, most notably in northern Rio
364 Grande do Sul and western Bahia (also see Figure 2b). Soybeans in Mato Grosso experienced not only a
365 substantial area expansion but also considerable yield growth. Per-pixel uncertainty of soybean yields
366 (Figure 7b) showed that the uncertainty estimates were mostly between 300 kg/ha to 500 kg/ha.
367 Moreover, the uncertainty distribution varied both spatially and temporally, with the south region (e.g.
368 Rio Grande do Sul) appeared to have slightly higher uncertainties than center west (e.g. Mato Grosso).

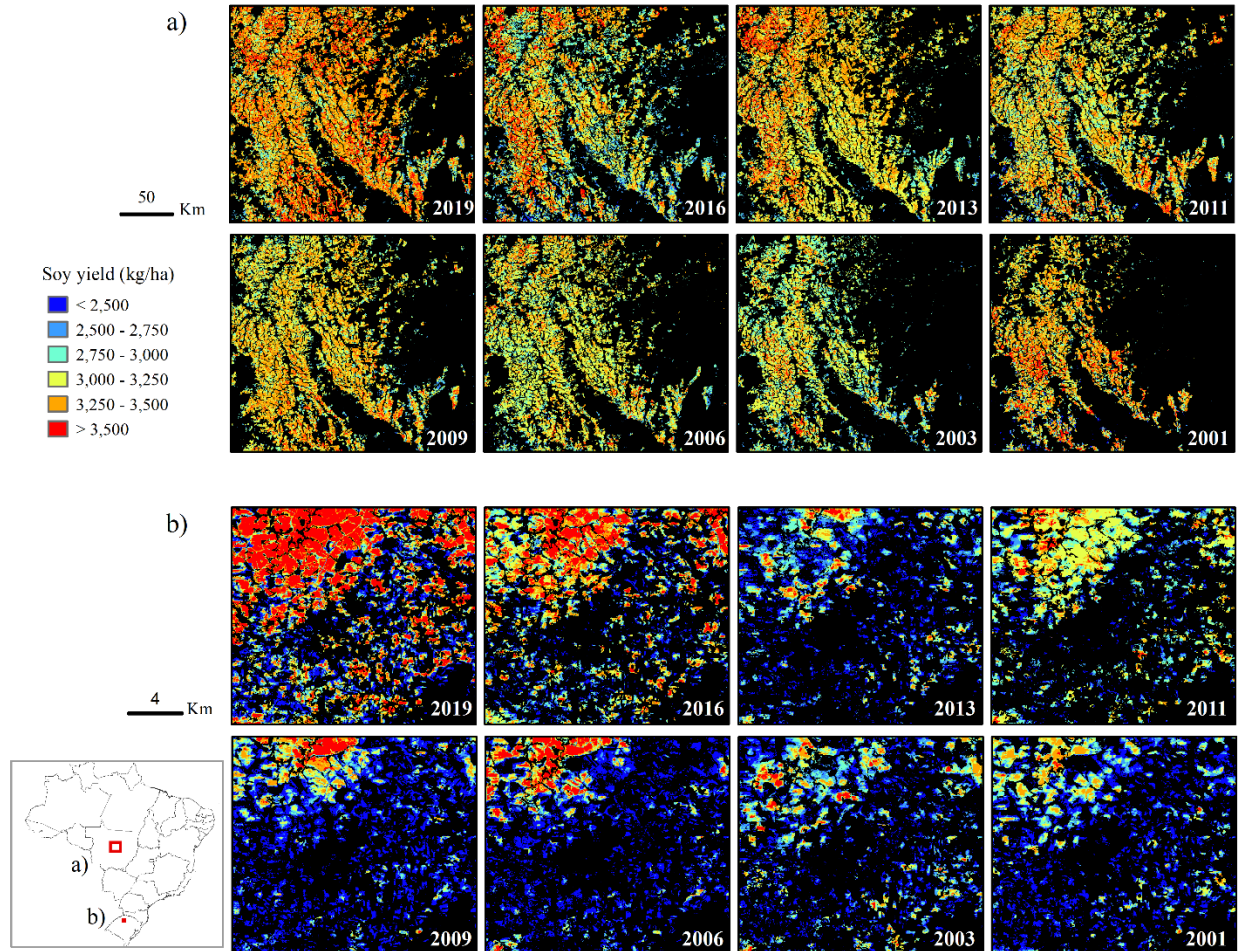


369

370 **Figure 7.** Annual soybean yield and uncertainty maps for selected years over Brazil. Yield and
 371 uncertainty maps were produced at 30 m spatial resolution and averaged to 1 km for the purpose of
 372 display. Regional details at 30 m resolution are shown in Figure 8.

373

374 The annual, 30 m resolution maps revealed field-level heterogeneity in soybean yields (Figure 8). Large
 375 contiguous soybean fields in central Mato Grosso have moderate-to-high yield and small variations
 376 between fields (Figure 8a), whereas smaller fragmented fields in Rio Grande do Sul show much larger
 377 variations (Figure 8b). Over the past 19 years, soybean yields in central Mato Grosso experienced an
 378 overall increase in most fields, whereas in Rio Grande do Sul, larger fields appeared to have relatively
 379 greater yield growth than smaller fields (Figure 8b).



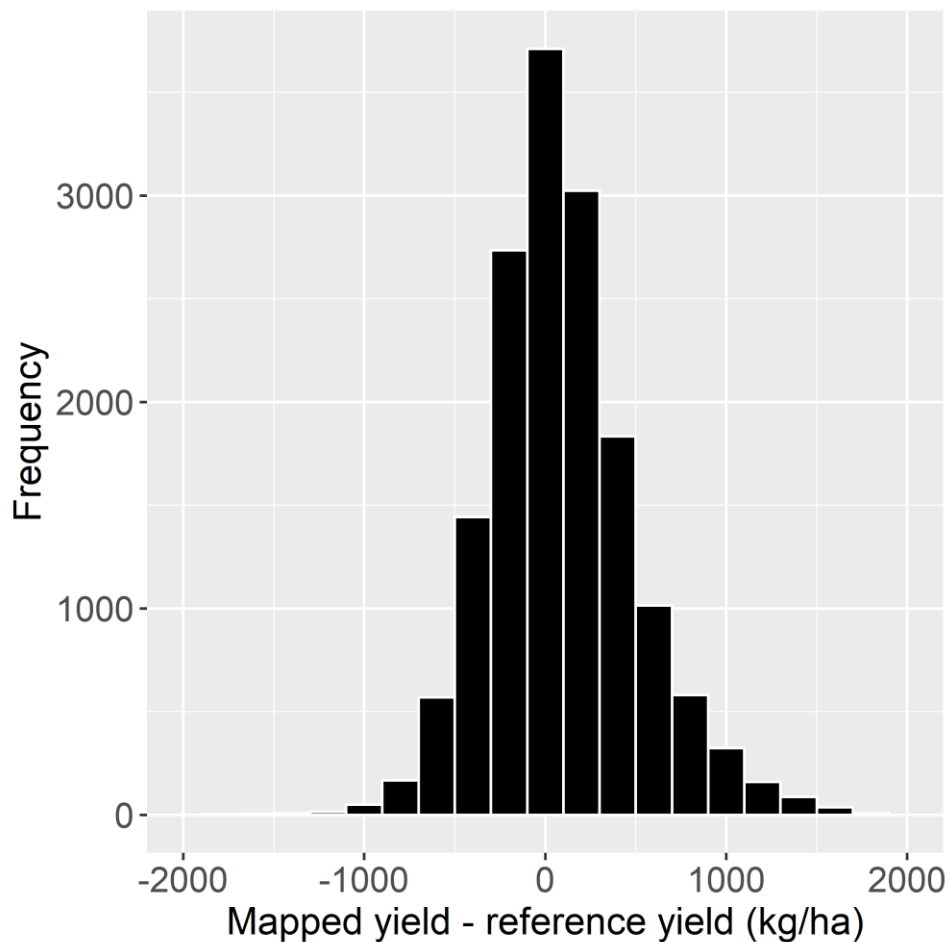
380

381 **Figure 8.** Spatial and temporal details of soybean yield at 30 m resolution in two selected regions: **a)**
 382 central Mato Grosso and **b)** northern Rio Grande do Sul. Field-level yield heterogeneity is revealed by the
 383 time series of high-resolution maps.

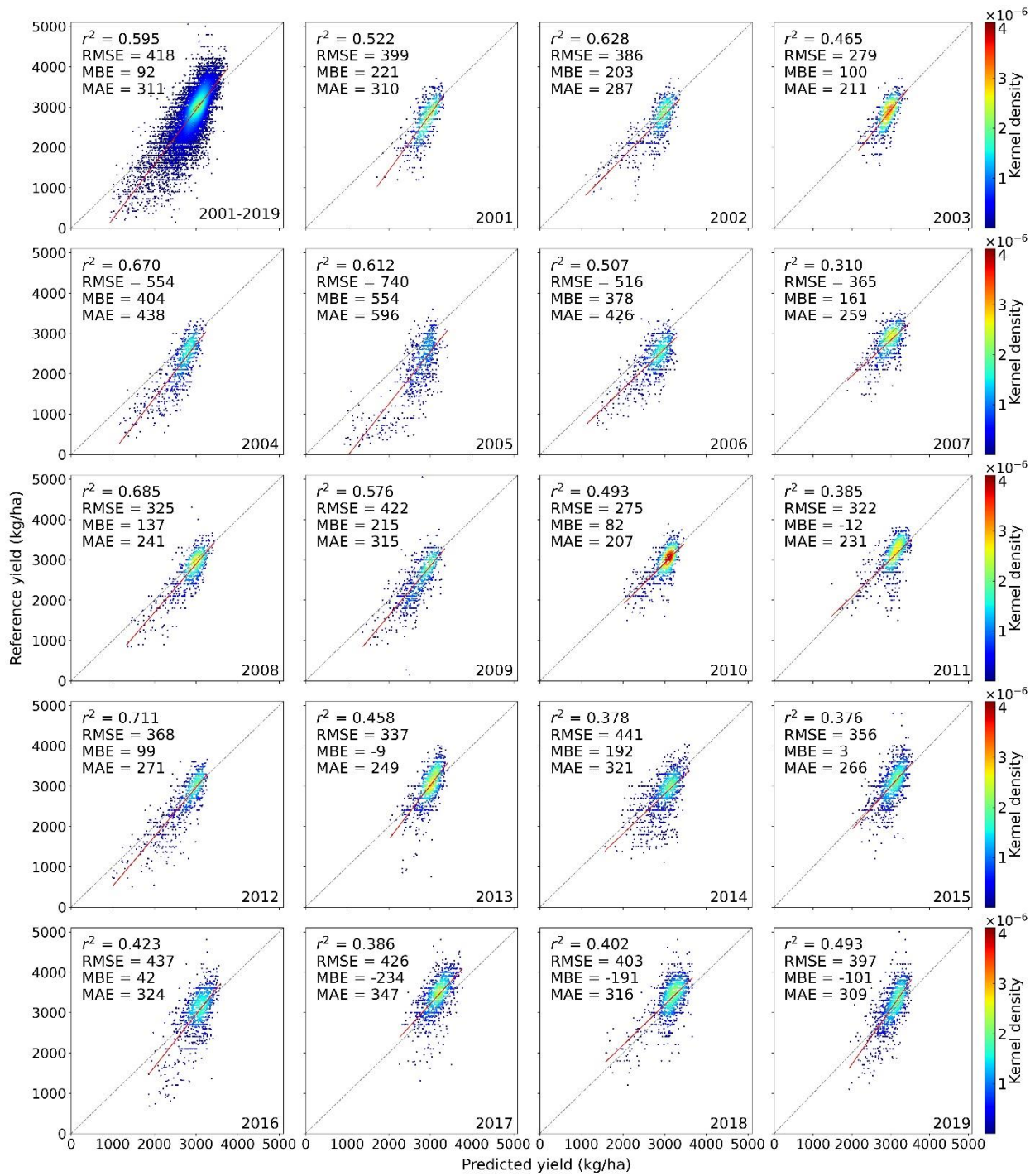
384 3.3. Map evaluation

385 The annual 30 m soybean yield maps were aggregated to municipal scale for a quantitative quality
 386 assessment. Compared to the reference data from official statistics, the yield map product had an overall
 387 RMSE of 418 kg/ha, a MAE of 311 kg/ha, an MBE of 92 kg/ha, and an r^2 of 0.60. Compared to the 2001-
 388 2019 national average yield of 2,869 kg/ha, the RMSE represents 15% error. These error metrics were all
 389 slightly worse than the model performance, with the RMSE about 20% higher (compared to 344 kg/ha;
 390 see detailed numbers of other error metrics in Figure 4). An overall slight positive bias was noted (mean
 391 bias of 92 kg/ha or 3% error compared to long-term average yield, Figure 9). Moreover, systematic

392 underestimation was still noticed at the high end of yield and overestimation at the low end of yield
 393 (Figure 10), although a linear regression successfully corrected model bias at the training stage at the
 394 municipal level (Figure 4). At the annual time scale, the map accuracy was comparable to model
 395 performance for the majority of the 19 years (Figure 10). The comparison between model performance
 396 and map quality assessment suggested that uncertainties at the 30 m pixel scale were larger than those at
 397 the aggregated municipal scale, highlighting a general multi-scale issue in the applications of regression-
 398 based machine learning algorithms in remote sensing.



399
 400 **Figure 9.** Histogram of the difference between predicted yield and reference yield at the municipal level
 401 between 2001 and 2019 (n=15,784) indicating a slight positive bias in the predicted yield.



402

403 **Figure 10.** Quality assessment of 30 m soybean yield maps for every year between 2001 and 2019. The
 404 annual maps were averaged to the municipal scale to derive predicted yields (x-axis). Reference yields (y-
 405 axis) are official statistics.

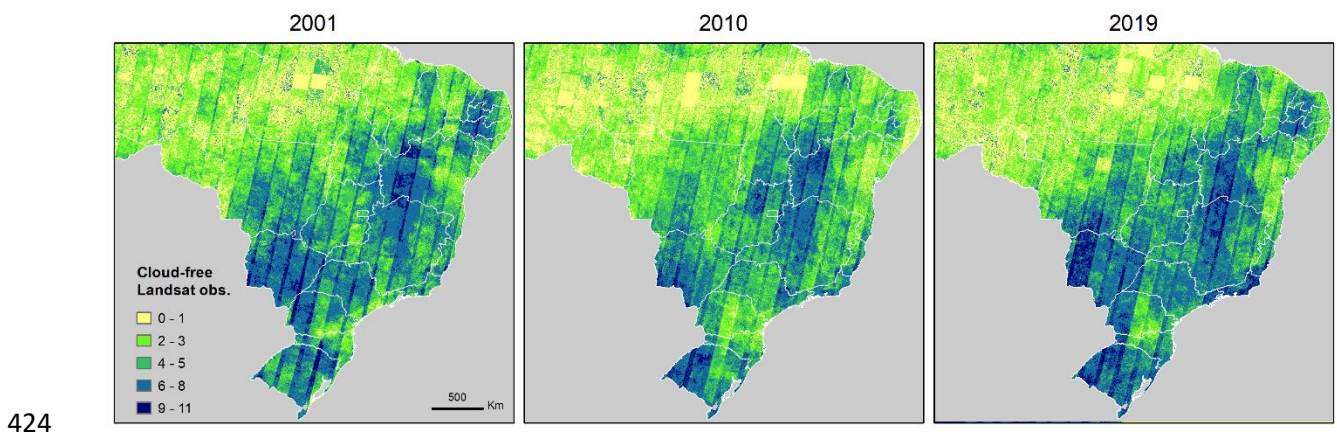
406

407 **4. Discussion**

408 **4.1. Uncertainty sources for yield modeling**

409 Model performance and the quality of the annual yield maps are influenced by a number of factors,
410 including the temporal density of satellite observations, the coarse spatial resolution and uncertainties of
411 climate and weather variables, lack of up-to-date soil measurements, unknown uncertainties in the official
412 statistics, lack of field-level reference data, missclassifications in the annual soybean masks, and the multi-
413 scale modeling and prediction procedure. The impacts of these factors are discussed in detail as follows.

414 Depending on the type of cultivar, environmental conditions and agricultural management practices,
415 soybean plants take 90 to 150 days from planting to maturity. During this short growing window,
416 vegetation cover in the field experiences rapid transitions from bare ground to nearly closed canopy and
417 to bare ground again. Such phenological dynamics require dense time-series data to capture the key
418 growth stages that are critical to crop biomass accumulation and yield formation. Studies have
419 demonstrated that the peak growing period in vegetation index is most important for modeling yield for
420 wheat, corn and soybeans (Becker-Reshef et al. 2010; Johnson 2014). In addition, natural disasters during
421 or after the seed-filling stage can cause severe yield reduction (Hosseini et al. 2020). In this study, we
422 used MODIS and Landsat as the main remote sensing data source. Due to the sparse temporal interval of
423 Landsat, cloud-free Landsat observations vary considerably in space and time (Figure 11).



425 **Figure 11.** Cloud-free Landsat observations between November 1st and April 30th in selected years over
426 Brazil.

427

428 On the other hand, daily MODIS acquisitions are more robust to cloud contamination. Indeed, the
429 important features identified by random forests include many MODIS-based spectral features. The most
430 important feature of the random forests model (model #1) was “M_NDVI_av90max”, which represented
431 the average value of the 90th percentile and maximum NDVI (i.e. peak NDVI) derived from MODIS
432 (Figure 12). The second and third most important features were MODIS-based peak-season NIR
433 reflectance and middle-season NDVI, respectively. These top three features accounted for >40% of
434 cumulative feature importance (Figure 12). Another inherent factor that enabled MODIS to be an efficient
435 sensor for modeling soybean yield is the large field size in Brazil (Fritz et al. 2015). The feature ranking
436 analysis suggested that improving the temporal density of high spatial resolution satellite data, such as the
437 Harmonized Landsat and Sentinel-2 product (Claverie et al. 2018), may improve yield mapping at the
438 field scale. Further research is also needed to investigate the utility of other freely available satellite data,
439 particularly radar data (e.g. Sentinel 1) for yield estimation, as radar data can provide complementary
440 information to optical data for crop monitoring (Song et al. 2021b; Veloso et al. 2017) in addition to their
441 all-weather data acquisition.

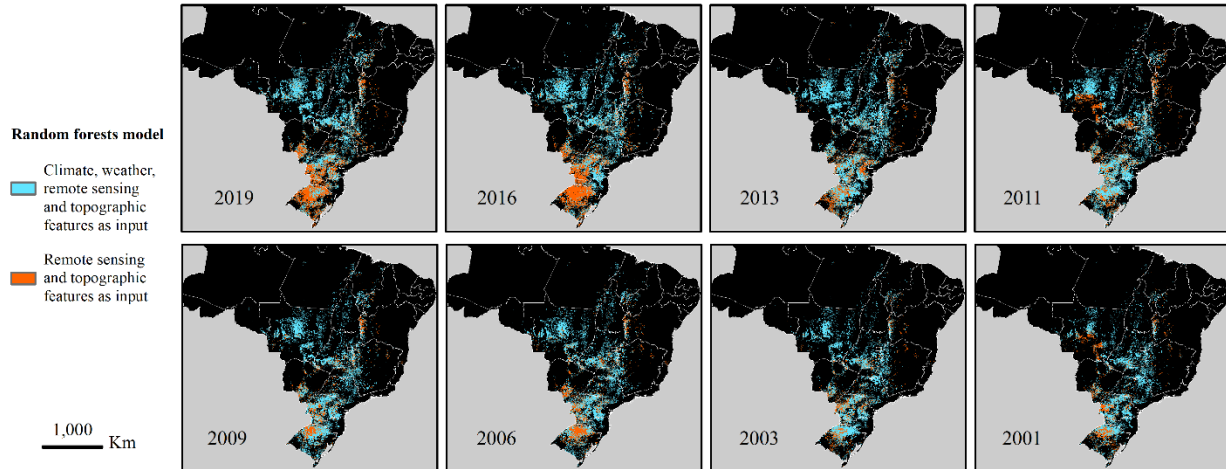
450 Our study explicitly demonstrated the value of climate and weather data for modeling crop yield. For the
 451 trained random forests model with all the features as input, climate and weather variables accounted for
 452 36% of the total feature importance (Table 2). Compared to the models with only remote sensing data as
 453 input, adding climate and weather variables reduced RMSE by about 7 to 9%, and the improvement was
 454 statistically significant. However, adding coarse-resolution climate and weather variables could also
 455 introduce undesirable artifacts. By constructing two models and through per-pixel composition of model
 456 outputs, our strategy effectively combined the advantages of the two respective models. For any given
 457 year, the primary model (i.e. the one with climate and weather variables as input) was chosen for the
 458 majority of soybean growing regions of the country, while the secondary model (i.e. the one without
 459 climate and weather variables) was selected only for some clustered regions (Figure 13). This data-driven
 460 approach relied on the explicit uncertainty outputs associated with predictions of random forests, and the
 461 composited map had minimum uncertainties from the multi-model ensemble. Future research will
 462 evaluate the uncertainty of climate and weather variables to yield estimation, and incorporate higher-
 463 resolution weather dataset for improved yield estimation, e.g. the Climate Hazards Group Infrared
 464 Precipitation with Stations (CHIRPS) precipitation data (Funk et al. 2015).

465

466 **Table 2.** Importance of the five categories of input variables in random forests model for soybean yield
 467 prediction. Details of the variables are listed in Table 1. The total importance of all variables within each
 468 category was calculated and reported.

Category of variables	Importance in random forests model
Landsat-based	0.1883
MODIS-based	0.4371
Climate	0.1037
Weather	0.2539
Topographic	0.0041
Soil	0.0128

469



470

471 **Figure 13.** Maps of random forests models chosen for predicting annual soybean yield. The model with
 472 climate and weather variables as input was more accurate and was used in the majority of the soybean
 473 growing regions of the country in every year.

474

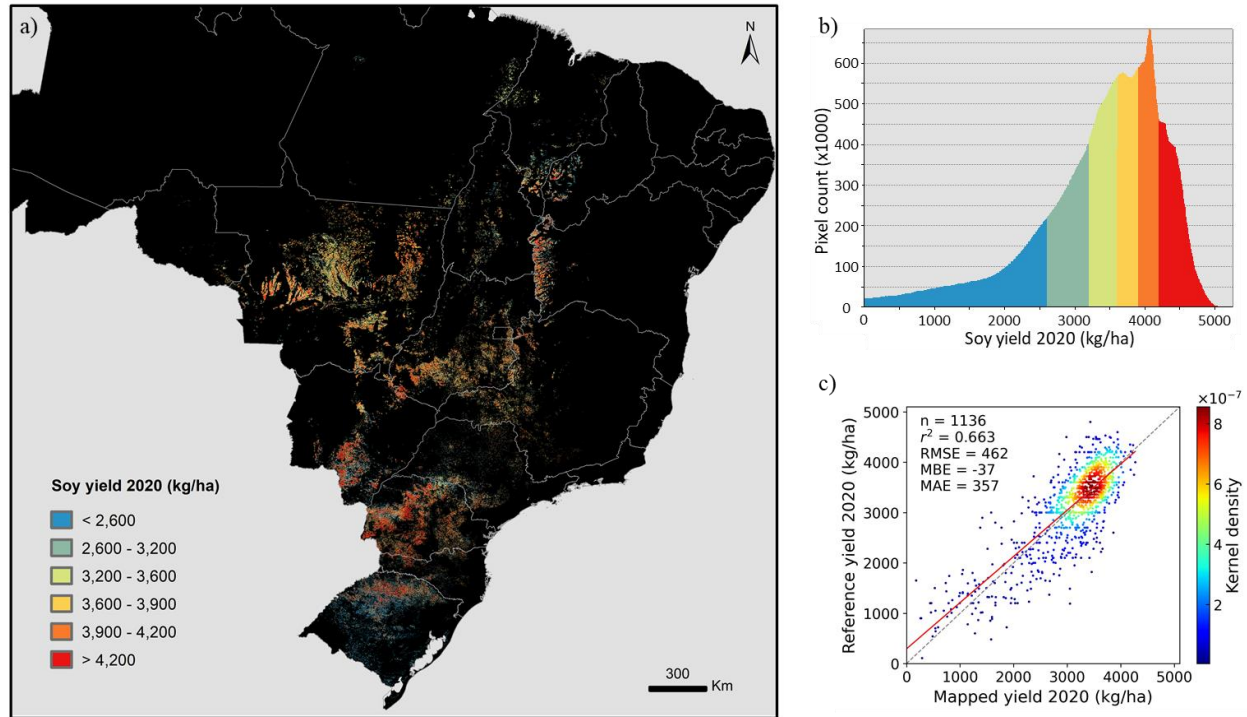
475 The lack of contribution by soil variables to soybean yield modeling was likely because the soil data were
 476 outdated. Soil characteristics and topography are strong determinant of cropland suitability (Ishikawa and
 477 Yamazaki 2021). We used the Harmonized World Soil Database (HWSD) in this study, which was
 478 compiled from multiple data sources (FAO/IIASA/ISRIC/ISSCAS/JRC 2012). The data source for Brazil
 479 was the Soil and Terrain database for Latin America and the Caribbean, at the scale of 1:5 million and
 480 released in 1998. Therefore, HWSD represents the soil conditions in Brazil before 1998. From 2000 to
 481 2019, soybean cultivation area in Brazil nearly tripled, and new soybean fields were mostly converted
 482 from pasture and forests (Song et al. 2021a). The conversion process involves removal of surface
 483 vegetation and extraction of the root systems. Subsequently, soil preparation is critical for cultivating
 484 soybeans on the newly converted land. In the Cerrado, the largest soybean growing biome in Brazil, the
 485 native soil condition is poor for crop production. Most of the soils in the Cerrado are highly weathered
 486 Oxisols and Ultisols, with high acidity and serious deficiency in nutrients (Lopes 1996). Improved
 487 management practices such as liming and fertilization have greatly increased soil fertility for growing

488 soybeans (Lopes 1996). These important changes in soil property are not reflected by the HWSD soil
489 database — likely the principal reason why the soil data did not contribute to soybean yield modeling.
490 Crop modeling studies suggest that soil-related yield variability outweighs the simulated year-to-year
491 variations in yield due to weather when no fertilizer is applied (Folberth et al., 2016). Up-to-date high-
492 quality soil data may improve modeling yielded for soybean and other crops in the tropics where agriculture
493 is expanding (Eigenbrod et al. 2020). Future studies will investigate the utility of higher resolution soil
494 dataset for yield mapping (Hengl et al. 2017). Generating other spatially explicit data on agricultural
495 management that are important for crop production such as seed variety and fertilizer use, is another
496 potential way of improving yield mapping.

497 Lastly, a common practice in crop yield mapping is to construct a machine learning model at an
498 aggregated spatial scale where public yield statistics are available, and apply the model to a finer scale at
499 which remote sensing data are acquired (e.g. Johnson 2014). The upscaling process (e.g. spatial
500 aggregation from pixel to municipal) can reduce uncertainties in the original data, as pixel-level errors
501 may be averaged out. Our yield models were calibrated at the municipal scale. More problematic is the
502 downscaling process (i.e. applying the trained model to pixels), as pixel-level errors often exist from e.g.
503 atmospheric correction or misclassification. The discrepancy between model performance (Figure 5,
504 overall RMSE 344 kg/ha) and yield map assessment at the same municipality scale (Figure 10, overall
505 RMSE 418 kg/ha) revealed a positive bias in the predicted yield (Figure 9), although the models were
506 unbiased after linear adjustment (Figure 4). This bias was primarily stemmed from the downscaling
507 process, where pixel-level errors could corrupt the results. Such bias may be removed using field-based
508 yield measurements. However, such datasets are traditionally held by private industry without public
509 access especially over large areas such as the national scale (see Deines et al. (2021) for the case of the
510 United States). Open access to field observations is rare in most parts of the world (Coutu et al. 2020).
511 Increasing the access to historical field observations is a potentially effective way of advancing crop yield
512 research.

4.2. Towards operational yield mapping

513
514 Achieving operational yield prediction using satellite data alone is a cost-effective approach of generating
515 timely information on crop production. To demonstrate the predictive capability of our yield models, we
516 applied the models, trained on 2001-2019 data, to 2020 data and produced a 30 m resolution soybean
517 yield map for 2020 (Figure 14). We also collected municipal yield statistics for 2020 and compared with
518 our 2020 yield map. Our random forests models, trained on 2001-2019 data, were able to predict 2020
519 yield with comparable accuracy as the withheld 2001-2019 test data. The RMSE, MBE and r^2 of the
520 direct output of random forests predictions for 2020 was 555 kg/ha, -145 kg/ha and 0.66, respectively.
521 Consistent with the model performance on 2001-2019 test data, an overall bias was noted. To eliminate
522 this bias, we applied the linear regression approach as reported above. We randomly selected 3% of
523 municipalities (n=34) from the 1,136 municipalities, and constructed a linear regression model using the
524 random forests-predicted yield as the independent variable and the 2020 municipal yield statistics as the
525 dependent variable. After bias correction, the MBE was reduced to -37 kg/ha, and RMSE was reduced to
526 462 kg/ha (Figure 14b). The RMSE represents 13% error relative to the national average of 3480 kg/ha in
527 2020. This result suggests that our pre-trained models can be used to generate high-resolution soybean
528 yield maps for future years with the caveat that a small amount of reference data are still needed for the
529 final bias correction. Given the continued operational satellite data acquisitions, including Landsat 8,
530 Landsat 9, MODIS and Visible Infrared Imaging Radiometer Suite (VIIRS), the demonstrated predictive
531 capability of our pre-trained yield models may be used for future yield mapping in a semi-operational
532 mode.



533

534 **Figure 14.** Soybean yield in year 2020 predicted using models trained on 2001-2019 data. a) 30-m map of
 535 soy yield 2020. b) Density distribution of the soy yield map. The colors match those shown on the map,
 536 and each color corresponds to approximately 1/6 of the total soy pixels. c) Comparison between predicted
 537 yield and municipal yield statistics as reference.

538

539 The rapidly developing technology of satellite remote sensing is transforming global agriculture. Earth
 540 observation data are increasingly used in research and operational settings for mapping crop types,
 541 monitoring crop growth, improving agricultural management and forecasting food production. Increasing
 542 the comprehensiveness within a single data product, including area, yield, cropping intensity and
 543 calendar, at high spatial and temporal resolution has been identified as one of the future research areas in
 544 developing global gridded cropping system data product (Kim et al. 2021). We showed in a previous
 545 study that satellite data could be used retrospectively mapping soybean over South America since 2001
 546 (Song et al. 2021a). Our 30 m South America soybean map product is being updated at an annual
 547 frequency in an operational mode as new satellite data are acquired. This study extends our research from

548 crop type mapping to yield mapping, and we demonstrated that pre-trained machine learning models
549 could be applied for yield mapping in future years. Our current approach for yield mapping and updating
550 uses satellite data of the entire growing season as input. This post-season mapping can generate highly
551 reliable data products, but lacks sufficient timeliness to capture production shocks resulted from e.g.
552 extreme weather events within the growing season. Recent research has demonstrated that early- and in-
553 season crop type mapping and crop yield forecasting could be achieved using advanced machine learning
554 algorithms (e.g. Lin et al. 2022), seasonal climate forecast (Iizumi et al. 2021), and in-season weather
555 observations (Schauberger et al. 2017). Implementing robust in-season forecasting methods in monitoring
556 systems is needed to mitigate the adverse impacts of climate change (Fritz et al. 2019; Kim et al. 2021; Li
557 et al. 2019; Lobell and Burke 2010; Nakalembe et al. 2021).

558 **5. Conclusions**

559 We developed a machine learning-based approach to map annual soybean yield in Brazil over the past
560 two decades. Consistent satellite observations from the open Landsat and MODIS data archives were used
561 to calibrate unbiased yield models using random forests followed by linear regression. Soybean yield
562 maps were generated at 30-meter spatial resolution for every year from 2001 to 2020. NDVI at the peak
563 of the growing season was found to be the most important variable for modeling soybean yield. Our study
564 explicitly demonstrated the utility of climate and weather variables for crop yield estimation. Our multi-
565 scale approach was effective in integrating official yield statistics at political unit level with remote
566 sensing data. Our study demonstrated that models trained on long-term historical data could be employed
567 to predict yield for future years. Our research also highlights that improving the temporal density of high-
568 resolution satellite observations, and enhancing the accessibility to field-level yield measurements are
569 viable ways to improve crop yield mapping over large areas.

570

571

572 **Acknowledgements**

573 This research was supported by the start-up funding to X.P.S. from Texas Tech University. We thank
 574 Marcos Adami for collecting the yield statistics data used in this study. Satellite data used to create the
 575 yield maps were processed using the GLAD ARD tools <https://glad.umd.edu/ard/>.

576 **References**

- 577 Battude, M., Al Bitar, A., Morin, D., Cros, J., Huc, M., Marais Sicre, C., Le Dantec, V., & Demarez, V.
 578 (2016). Estimating maize biomass and yield over large areas using high spatial and temporal
 579 resolution Sentinel-2 like remote sensing data. *Remote Sensing of Environment*, *184*, 668-681
- 580 Becker-Reshef, I., Vermote, E., Lindeman, M., & Justice, C. (2010). A generalized regression-based
 581 model for forecasting winter wheat yields in Kansas and Ukraine using MODIS data. *Remote*
 582 *Sensing of Environment*, *114*, 1312-1323
- 583 Benami, E., Jin, Z., Carter, M.R., Ghosh, A., Hijmans, R.J., Hobbs, A., Kenduiywo, B., & Lobell, D.B.
 584 (2021). Uniting remote sensing, crop modelling and economics for agricultural risk management.
 585 *Nature Reviews Earth & Environment*, *2*, 140-159
- 586 Bolton, D.K., & Friedl, M.A. (2013). Forecasting crop yield using remotely sensed vegetation indices and
 587 crop phenology metrics. *Agricultural and Forest Meteorology*, *173*, 74-84
- 588 Breiman, L. (2001). Random Forests. *Machine Learning*, *45*, 5-32
- 589 Cai, Y., Guan, K., Lobell, D., Potgieter, A.B., Wang, S., Peng, J., Xu, T., Asseng, S., Zhang, Y., You, L.,
 590 & Peng, B. (2019). Integrating satellite and climate data to predict wheat yield in Australia using
 591 machine learning approaches. *Agricultural and Forest Meteorology*, *274*, 144-159
- 592 Claverie, M., Demarez, V., Duchemin, B., Hagolle, O., Ducrot, D., Marais-Sicre, C., Dejoux, J.-F., Huc,
 593 M., Keravec, P., Béziat, P., Fieuzal, R., Ceschia, E., & Dedieu, G. (2012). Maize and sunflower
 594 biomass estimation in southwest France using high spatial and temporal resolution remote sensing
 595 data. *Remote Sensing of Environment*, *124*, 844-857

- 596 Claverie, M., Ju, J., Masek, J.G., Dungan, J.L., Vermote, E.F., Roger, J.-C., Skakun, S.V., & Justice, C.
 597 (2018). The Harmonized Landsat and Sentinel-2 surface reflectance data set. *Remote Sensing of*
 598 *Environment*, 219, 145-161
- 599 Coutu, S., Becker-Reshef, I., Whitcraft, A.K., & Justice, C. (2020). Food security: underpin with public
 600 and private data sharing. *Nature*, 578, 515
- 601 de Wit, A., Boogaard, H., Fumagalli, D., Janssen, S., Knapen, R., van Kraalingen, D., Supit, I., van der
 602 Wijngaart, R., & van Diepen, K. (2019). 25 years of the WOFOST cropping systems model.
 603 *Agricultural Systems*, 168, 154-167
- 604 de Wit, A., Duveiller, G., & Defourny, P. (2012). Estimating regional winter wheat yield with WOFOST
 605 through the assimilation of green area index retrieved from MODIS observations. *Agricultural*
 606 *and Forest Meteorology*, 164, 39-52
- 607 Defourny, P., Bontemps, S., Bellemans, N., Cara, C., Dedieu, G., Guzzonato, E., Hagolle, O., Inglada, J.,
 608 Nicola, L., Rabaute, T., Savinaud, M., Udrou, C., Valero, S., Bégué, A., Dejoux, J.-F., El Harti,
 609 A., Ezzahar, J., Kussul, N., Labbassi, K., Lebourgeois, V., Miao, Z., Newby, T., Nyamugama, A.,
 610 Salh, N., Shelestov, A., Simonneaux, V., Traore, P.S., Traore, S.S., & Koetz, B. (2019). Near
 611 real-time agriculture monitoring at national scale at parcel resolution: Performance assessment of
 612 the Sen2-Agri automated system in various cropping systems around the world. *Remote Sensing*
 613 *of Environment*, 221, 551-568
- 614 DeFries, R.S., Field, C.B., Fung, I., Justice, C.O., Los, S., Matson, P.A., Matthews, E., Mooney, H.A.,
 615 Potter, C.S., Prentice, K., Sellers, P.J., Townshend, J.R.G., Tucker, C.J., Ustin, S.L., & Vitousek,
 616 P.M. (1995). Mapping the land surface for global atmosphere-biosphere models: Toward
 617 continuous distributions of vegetation's functional properties. *Journal of Geophysical Research:*
 618 *Atmospheres*, 100, 20867-20882.

- 619 Deines, J.M., Patel, R., Liang, S.-Z., Dado, W., & Lobell, D.B. (2021). A million kernels of truth: Insights
 620 into scalable satellite maize yield mapping and yield gap analysis from an extensive ground
 621 dataset in the US Corn Belt. *Remote Sensing of Environment*, 253, 112174
- 622 Delécolle, R., Maas, S., Guerif, M., & Baret, F. (1992). Remote sensing and crop production models:
 623 present trends. *ISPRS Journal of Photogrammetry and Remote Sensing*, 47, 145-161
- 624 Doraiswamy, P.C., Hatfield, J.L., Jackson, T.J., Akhmedova, B., Prueger, J., & Sterna, A. (2004).
 625 Crop condition and yield simulations using Landsat and MODIS. *Remote Sensing of*
 626 *Environment*, 92, 548-559
- 627 Duchemin, B., Maisongrande, P., Boulet, G., & Benhadj, I. (2008). A simple algorithm for yield
 628 estimates: Evaluation for semi-arid irrigated winter wheat monitored with green leaf area index.
 629 *Environmental Modelling & Software*, 23, 876-892
- 630 Eigenbrod, F., Beckmann, M., Dunnett, S., Graham, L., Holland, R.A., Meyfroidt, P., Seppelt, R., Song,
 631 X.P., Spake, R., Vaclavik, T., & Verburg, P.H. (2020). Identifying Agricultural Frontiers for
 632 Modeling Global Cropland Expansion. *One Earth*, 3, 504-514
- 633 FAO (2020). FAOSTAT database. In. Rome: FAO
- 634 FAO/IIASA/ISRIC/ISSCAS/JRC (2012). Harmonized World Soil Database (version 1.2). In. FAO,
 635 Rome, Italy and IIASA, Laxenburg, Austria.
- 636 Folberth, C., Skalsky, R., Moltchanova, E., Balkovic, J., Azevedo, L.B., Obersteiner, M., & van der
 637 Velde, M. (2016). Uncertainty in soil data can outweigh climate impact signals in global crop
 638 yield simulations. *Nat Commun*, 7, 11872
- 639 Franch, B., Vermote, E.F., Becker-Reshef, I., Claverie, M., Huang, J., Zhang, J., Justice, C., & Sobrino,
 640 J.A. (2015). Improving the timeliness of winter wheat production forecast in the United States of
 641 America, Ukraine and China using MODIS data and NCAR Growing Degree Day information.
 642 *Remote Sensing of Environment*, 161, 131-148
- 643 Fritz, S., See, L., Bayas, J.C.L., Waldner, F., Jacques, D., Becker-Reshef, I., Whitcraft, A., Baruth, B.,
 644 Bonifacio, R., Crutchfield, J., Rembold, F., Rojas, O., Schucknecht, A., Van der Velde, M.,

- 645 Verdin, J., Wu, B., Yan, N., You, L., Gilliams, S., Mücher, S., Tetrault, R., Moorthy, I., &
 646 McCallum, I. (2019). A comparison of global agricultural monitoring systems and current gaps.
 647 *Agricultural Systems*, *168*, 258-272
- 648 Fritz, S., See, L., McCallum, I., You, L., Bun, A., Moltchanova, E., Duerauer, M., Albrecht, F., Schill, C.,
 649 Perger, C., Havlik, P., Mosnier, A., Thornton, P., Wood-Sichra, U., Herrero, M., Becker-Reshef,
 650 I., Justice, C., Hansen, M., Gong, P., Abdel Aziz, S., Cipriani, A., Cumani, R., Cecchi, G.,
 651 Conchedda, G., Ferreira, S., Gomez, A., Haffani, M., Kayitakire, F., Malanding, J., Mueller, R.,
 652 Newby, T., Nonguierma, A., Olusegun, A., Ortner, S., Rajak, D.R., Rocha, J., Schepaschenko, D.,
 653 Schepaschenko, M., Terekhov, A., Tiangwa, A., Vancutsem, C., Vintrou, E., Wenbin, W., van
 654 der Velde, M., Dunwoody, A., Kraxner, F., & Obersteiner, M. (2015). Mapping global cropland
 655 and field size. *Glob Chang Biol*, *21*, 1980-1992
- 656 Funk, C., & Budde, M.E. (2009). Phenologically-tuned MODIS NDVI-based production anomaly
 657 estimates for Zimbabwe. *Remote Sensing of Environment*, *113*, 115-125
- 658 Funk, C., Peterson, P., Landsfeld, M., Pedreros, D., Verdin, J., Shukla, S., Husak, G., Rowland, J.,
 659 Harrison, L., Hoell, A., & Michaelsen, J. (2015). The climate hazards infrared precipitation with
 660 stations--a new environmental record for monitoring extremes. *Sci Data*, *2*, 150066
- 661 Gallego, F.J. (2004). Remote sensing and land cover area estimation. *International Journal of Remote*
 662 *Sensing*, *25*, 3019-3047
- 663 Gao, F., Anderson, M., Daughtry, C., & Johnson, D. (2018). Assessing the Variability of Corn and
 664 Soybean Yields in Central Iowa Using High Spatiotemporal Resolution Multi-Satellite Imagery.
 665 *Remote Sensing*, *10*, 1489.
- 666 Gibbs, H.K., Ruesch, A.S., Achard, F., Clayton, M.K., Holmgren, P., Ramankutty, N., & Foley, J.A.
 667 (2010). Tropical forests were the primary sources of new agricultural land in the 1980s and
 668 1990s. *Proceedings of the National Academy of Sciences, USA*, *107*, 16732-16737
- 669 Gitelson, A.A. (2004). Wide Dynamic Range Vegetation Index for remote quantification of biophysical
 670 characteristics of vegetation. *Journal of Plant Physiology*, *161*, 165-173

- 671 González-Alonso, F., & Cuevas, J.M. (1993). Remote sensing and agricultural statistics: crop area
 672 estimation through regression estimators and confusion matrices. *International Journal of Remote*
 673 *Sensing, 14*, 1215-1219
- 674 Gorelick, N., Hancher, M., Dixon, M., Ilyushchenko, S., Thau, D., & Moore, R. (2017). Google Earth
 675 Engine: Planetary-scale geospatial analysis for everyone. *Remote Sensing of Environment, 202*,
 676 18-27
- 677 Hansen, M.C., Potapov, P.V., Moore, R., Hancher, M., Turubanova, S.A., Tyukavina, A., Thau, D.,
 678 Stehman, S.V., Goetz, S.J., Loveland, T.R., & Kommareddy, A. (2013). High-resolution global
 679 maps of 21st-century forest cover change. *Science, 342*, 850-853.
- 680 Harris, I., Osborn, T.J., Jones, P., & Lister, D. (2020). Version 4 of the CRU TS monthly high-resolution
 681 gridded multivariate climate dataset. *Sci Data, 7*, 109
- 682 Hengl, T., Mendes de Jesus, J., Heuvelink, G.B., Ruiperez Gonzalez, M., Kilibarda, M., Blagotic, A.,
 683 Shangguan, W., Wright, M.N., Geng, X., Bauer-Marschallinger, B., Guevara, M.A., Vargas, R.,
 684 MacMillan, R.A., Batjes, N.H., Leenaars, J.G., Ribeiro, E., Wheeler, I., Mantel, S., & Kempen,
 685 B. (2017). SoilGrids250m: Global gridded soil information based on machine learning. *PLoS*
 686 *One, 12*, e0169748
- 687 Holzworth, D.P., Huth, N.I., deVoil, P.G., Zurcher, E.J., Herrmann, N.I., McLean, G., Chenu, K., van
 688 Oosterom, E.J., Snow, V., Murphy, C., Moore, A.D., Brown, H., Whish, J.P.M., Verrall, S.,
 689 Fainges, J., Bell, L.W., Peake, A.S., Poulton, P.L., Hochman, Z., Thorburn, P.J., Gaydon, D.S.,
 690 Dalgliesh, N.P., Rodriguez, D., Cox, H., Chapman, S., Doherty, A., Teixeira, E., Sharp, J.,
 691 Cichota, R., Vogeler, I., Li, F.Y., Wang, E., Hammer, G.L., Robertson, M.J., Dimes, J.P.,
 692 Whitbread, A.M., Hunt, J., van Rees, H., McClelland, T., Carberry, P.S., Hargreaves, J.N.G.,
 693 MacLeod, N., McDonald, C., Harsdorf, J., Wedgwood, S., & Keating, B.A. (2014). APSIM –
 694 Evolution towards a new generation of agricultural systems simulation. *Environmental Modelling*
 695 *& Software, 62*, 327-350

- 696 Hosseini, M., Kerner, H.R., Sahajpal, R., Puricelli, E., Lu, Y.-H., Lawal, A.F., Humber, M.L., Mitkish,
 697 M., Meyer, S., & Becker-Reshef, I. (2020). Evaluating the Impact of the 2020 Iowa Derecho on
 698 Corn and Soybean Fields Using Synthetic Aperture Radar. *Remote Sensing*, *12*, 3878
- 699 Hu, Q., Yin, H., Friedl, M.A., You, L., Li, Z., Tang, H., & Wu, W. (2021). Integrating coarse-resolution
 700 images and agricultural statistics to generate sub-pixel crop type maps and reconciled area
 701 estimates. *Remote Sensing of Environment*, *258*, 112365
- 702 Huang, J., Tian, L., Liang, S., Ma, H., Becker-Reshef, I., Huang, Y., Su, W., Zhang, X., Zhu, D., & Wu,
 703 W. (2015). Improving winter wheat yield estimation by assimilation of the leaf area index from
 704 Landsat TM and MODIS data into the WOFOST model. *Agricultural and Forest Meteorology*,
 705 *204*, 106-121
- 706 Huang, X., Schneider, A., & Friedl, M.A. (2016). Mapping sub-pixel urban expansion in China using
 707 MODIS and DMSP/OLS nighttime lights. *Remote Sensing of Environment*, *175*, 92-108
- 708 Iizumi, T., Shin, Y., Choi, J., van der Velde, M., Nisini, L., Kim, W., & Kim, K.-H. (2021). Evaluating
 709 the 2019 NARO-APCC Joint Crop Forecasting Service Yield Forecasts for Northern Hemisphere
 710 Countries. *Weather and Forecasting*, *36*, 879-891
- 711 Ines, A.V.M., Das, N.N., Hansen, J.W., & Njoku, E.G. (2013). Assimilation of remotely sensed soil
 712 moisture and vegetation with a crop simulation model for maize yield prediction. *Remote Sensing*
 713 *of Environment*, *138*, 149-164
- 714 Ishikawa, Y., & Yamazaki, D. (2021). Global high-resolution estimation of cropland suitability and its
 715 comparative analysis to actual cropland distribution. *Hydrological Research Letters*, *15*, 9-15
- 716 Jin, X., Kumar, L., Li, Z., Feng, H., Xu, X., Yang, G., & Wang, J. (2018). A review of data assimilation
 717 of remote sensing and crop models. *European Journal of Agronomy*, *92*, 141-152
- 718 Jin, Z., Azzari, G., You, C., Di Tommaso, S., Aston, S., Burke, M., & Lobell, D.B. (2019). Smallholder
 719 maize area and yield mapping at national scales with Google Earth Engine. *Remote Sensing of*
 720 *Environment*, *228*, 115-128

- 721 Johnson, D.M. (2014). An assessment of pre- and within-season remotely sensed variables for forecasting
 722 corn and soybean yields in the United States. *Remote Sensing of Environment*, *141*, 116-128
- 723 Johnson, M.D., Hsieh, W.W., Cannon, A.J., Davidson, A., & Bédard, F. (2016). Crop yield forecasting on
 724 the Canadian Prairies by remotely sensed vegetation indices and machine learning methods.
 725 *Agricultural and Forest Meteorology*, *218-219*, 74-84
- 726 Jones, J.W., Hoogenboom, G., Porter, C.H., Boote, K.J., Batchelor, W.D., Hunt, L.A., Wilkens, P.W.,
 727 Singh, U., Gijssman, A.J., & Ritchie, J.T. (2003). The DSSAT cropping system model. *European*
 728 *Journal of Agronomy*, *18*, 235–265
- 729 Kang, Y., & Özdoğan, M. (2019). Field-level crop yield mapping with Landsat using a hierarchical data
 730 assimilation approach. *Remote Sensing of Environment*, *228*, 144-163
- 731 Kim, K.-H., Doi, Y., Ramankutty, N., & Iizumi, T. (2021). A review of global gridded cropping system
 732 data products. *Environmental Research Letters*, *16*
- 733 King, L., Adusei, B., Stehman, S., Potapov, P.V., Song, X.-P., Krylov, A., Bella, C.D., Loveland, T.R.,
 734 Johnson, D.M., & Hansen, M.C. (2017). A multi-resolution approach to national-scale cultivated
 735 area estimation of soybean. *Remote Sensing of Environment*, *195*, 13-29
- 736 Li, A., Liang, S., Wang, A., & Qin, J. (2007). Estimating crop yield from multi-temporal satellite data
 737 using multivariate regression and neural network techniques. *Photogrammetric Engineering &*
 738 *Remote Sensing*, *73*, 1149-1157
- 739 Li, X.-Y., Li, X., Fan, Z., Mi, L., Kandakji, T., Song, Z., Li, D., & Song, X.-P. (2022). Civil war hinders
 740 crop production and threatens food security in Syria. *Nature Food*, *3*, 38-46
- 741 Li, Y., Guan, K., Schnitkey, G.D., DeLucia, E., & Peng, B. (2019). Excessive rainfall leads to maize yield
 742 loss of a comparable magnitude to extreme drought in the United States. *Glob Chang Biol*, *25*,
 743 2325-2337
- 744 Liu, J., Huffman, T., Qian, B., Shang, J., Li, Q., Dong, T., Davidson, A., & Jing, Q. (2020). Crop yield
 745 estimation in the Canadian Prairies using Terra/MODIS-derived crop metrics. *IEEE Journal of*
 746 *Selected Topics in Applied Earth Observations and Remote Sensing*, *13*, 2685-2697

- 747 Lobell, D.B. (2013). The use of satellite data for crop yield gap analysis. *Field Crops Research*, 143, 56-
 748 64
- 749 Lobell, D.B., & Burke, M.B. (2010). On the use of statistical models to predict crop yield responses to
 750 climate change. *Agricultural and Forest Meteorology*, 150, 1443-1452
- 751 Lobell, D.B., Thau, D., Seifert, C., Engle, E., & Little, B. (2015). A scalable satellite-based crop yield
 752 mapper. *Remote Sensing of Environment*, 164, 324-333
- 753 Lopes, A.S. (1996). Soils under Cerrado: a success story in soil management. *Better crops international*,
 754 10, 10
- 755 Massey, R., Sankey, T.T., Congalton, R.G., Yadav, K., Thenkabail, P.S., Ozdogan, M., & Sánchez
 756 Meador, A.J. (2017). MODIS phenology-derived, multi-year distribution of conterminous U.S.
 757 crop types. *Remote Sensing of Environment*, 198, 490-503
- 758 Mateo-Sanchis, A., Piles, M., Muñoz-Mari, J., Adsuara, J.E., Perez-Suay, A., & Camps-Valls, G. (2019).
 759 Synergistic integration of optical and microwave satellite data for crop yield estimation. *Remote
 760 Sens Environ*, 234, 111460
- 761 Moulin, S., Bondeau, A., & Delecolle, R. (1998). Combining agricultural crop models and satellite
 762 observations: From field to regional scales. *International Journal of Remote Sensing*, 19, 1021-
 763 1036
- 764 Mulla, D.J. (2013). Twenty five years of remote sensing in precision agriculture: Key advances and
 765 remaining knowledge gaps. *Biosystems Engineering*, 114, 358-371
- 766 Nakalembe, C., Becker-Reshef, I., Bonifacio, R., Hu, G., Humber, M.L., Justice, C.J., Keniston, J.,
 767 Mwangi, K., Rembold, F., Shukla, S., Urbano, F., Whitcraft, A.K., Li, Y., Zappacosta, M., Jarvis,
 768 I., & Sanchez, A. (2021). A review of satellite-based global agricultural monitoring systems
 769 available for Africa. *Global Food Security*, 29
- 770 Nearing, G.S., Crow, W.T., Thorp, K.R., Moran, M.S., Reichle, R.H., & Gupta, H.V. (2012).
 771 Assimilating remote sensing observations of leaf area index and soil moisture for wheat yield
 772 estimates: An observing system simulation experiment. *Water Resources Research*, 48, W05525

- 773 Paudel, D., Boogaard, H., de Wit, A., Janssen, S., Osinga, S., Pylianidis, C., & Athanasiadis, I.N. (2021).
 774 Machine learning for large-scale crop yield forecasting. *Agricultural Systems*, 187, 103016
- 775 Potapov, P., Hansen, M.C., Kommareddy, I., Kommareddy, A., Turubanova, S., Pickens, A., Adusei, B.,
 776 Tyukavina, A., & Ying, Q. (2020). Landsat Analysis Ready Data for Global Land Cover and
 777 Land Cover Change Mapping. *Remote Sensing*, 12, 426
- 778 Potapov, P., Turubanova, S., Hansen, M.C., Tyukavina, A., Zalles, V., Khan, A., Song, X.-P., Pickens,
 779 A., Shen, Q., & Cortez, J. (2022). Global maps of cropland extent and change show accelerated
 780 cropland expansion in the twenty-first century. *Nature Food*, 3, 19-28
- 781 Sakamoto, T., Gitelson, A.A., & Arkebauer, T.J. (2013). MODIS-based corn grain yield estimation model
 782 incorporating crop phenology information. *Remote Sensing of Environment*, 131, 215-231
- 783 Schauburger, B., Gornott, C., & Wechsung, F. (2017). Global evaluation of a semiempirical model for
 784 yield anomalies and application to within-season yield forecasting. *Glob Chang Biol*, 23, 4750-
 785 4764
- 786 Schwalbert, R.A., Amado, T., Corassa, G., Pott, L.P., Prasad, P.V.V., & Ciampitti, I.A. (2020). Satellite-
 787 based soybean yield forecast: Integrating machine learning and weather data for improving crop
 788 yield prediction in southern Brazil. *Agricultural and Forest Meteorology*, 284, 107886
- 789 Shahhosseini, M., Hu, G., Huber, I., & Archontoulis, S.V. (2021). Coupling machine learning and crop
 790 modeling improves crop yield prediction in the US Corn Belt. *Sci Rep*, 11, 1606
- 791 Skakun, S., Franch, B., Vermote, E., Roger, J.-C., Becker-Reshef, I., Justice, C., & Kussul, N. (2017).
 792 Early season large-area winter crop mapping using MODIS NDVI data, growing degree days
 793 information and a Gaussian mixture model. *Remote Sensing of Environment*, 195, 244-258
- 794 Skakun, S., Kalecinski, N.I., Brown, M.G.L., Johnson, D.M., Vermote, E.F., Roger, J.-C., & Franch, B.
 795 (2021). Assessing within-Field Corn and Soybean Yield Variability from WorldView-3, Planet,
 796 Sentinel-2, and Landsat 8 Satellite Imagery. *Remote Sensing*, 13, 872
- 797 Song, X.-P., Hansen, M.C., Potapov, P.V., Adusei, B., Pickering, J., Adami, M., Lima, A., Zalles, V.,
 798 Stehman, S.V., Di Bella, C.M., Conde, M.C., Copati, E.J., Fernandes, L.B., Hernandez-Serna, A.,

- 799 Jantz, S.M., Pickens, A.H., Turubanova, S., & Tyukavina, A. (2021a). Massive soybean
800 expansion in South America since 2000 and implications for conservation. *Nature Sustainability*,
801 *4*, 784-792
- 802 Song, X.-P., Hansen, M.C., Stehman, S.V., Potapov, P.V., Tyukavina, A., Vermote, E.F., & Townshend,
803 J.R. (2018). Global land change from 1982 to 2016. *Nature*, *560*, 639-643
- 804 Song, X.-P., Huang, W., Hansen, M.C., & Potapov, P. (2021b). An evaluation of Landsat, Sentinel-2,
805 Sentinel-1 and MODIS data for crop type mapping. *Science of Remote Sensing*, *3*, 100018
- 806 Song, X.-P., Potapov, P.V., Krylov, A., King, L., Di Bella, C.M., Hudson, A., Khan, A., Adusei, B.,
807 Stehman, S.V., & Hansen, M.C. (2017). National-scale soybean mapping and area estimation in
808 the United States using medium resolution satellite imagery and field survey. *Remote Sensing of*
809 *Environment*, *190*, 383-395
- 810 Tucker, C.J., Holben, B., Elgin Jr, J., & McMurtrey III, J. (1980). Relationship of spectral data to grain
811 yield variation. *Photogrammetric Engineering and Remote Sensing*, *46*, 657-666
- 812 Veloso, A., Mermoz, S., Bouvet, A., Le Toan, T., Planells, M., Dejoux, J.-F., & Ceschia, E. (2017).
813 Understanding the temporal behavior of crops using Sentinel-1 and Sentinel-2-like data for
814 agricultural applications. *Remote Sensing of Environment*, *199*, 415-426
- 815 Vermote, E., & Wolfe, R. (2015). MOD09GQ MODIS/Terra Surface Reflectance Daily L2G Global
816 250m SIN Grid V006 [Data set]. NASA EOSDIS Land Processes DAAC. Accessed 2021-11-27
817 from <https://doi.org/10.5067/MODIS/MOD09GQ.006>
- 818 Vroege, W., Vrieling, A., & Finger, R. (2021). Satellite support to insure farmers against extreme
819 droughts. *Nature Food*, *2*, 215-217
- 820 Wardlow, B.D., & Egbert, S.L. (2008). Large-area crop mapping using time-series MODIS 250 m NDVI
821 data: An assessment for the U.S. Central Great Plains. *Remote Sensing of Environment*, *112*,
822 1096-1116
- 823 Weiss, M., Jacob, F., & Duveiller, G. (2020). Remote sensing for agricultural applications: A meta-
824 review. *Remote Sensing of Environment*, *236*

- 825 Wieder, W.R., Boehnert, J., Bonan, G.B., & Langseth, M. (2014). RegridDED Harmonized World Soil
826 Database v1.2. In: Oak Ridge National Laboratory Distributed Active Archive Center, Oak
827 Ridge, Tennessee, USA.
- 828 Williams, J., Jones, C., Kiniry, J., & Spanel, D.A. (1989). The EPIC crop growth model. *Transactions of*
829 *the ASAE*, 32, 497-0511
- 830 Yang, H.S., Dobermann, A., Lindquist, J.L., Walters, D.T., Arkebauer, T.J., & Cassman, K.G. (2004).
831 Hybrid-maize—a maize simulation model that combines two crop modeling approaches. *Field*
832 *Crops Research*, 87, 131-154
- 833 Zhang, G., & Lu, Y., (2012). Bias-corrected random forests in regression. *Journal of Applied Statistics*,
834 39, 151-160
- 835 Zalles, V., Hansen, M.C., Potapov, P.V., Parker, D., Stehman, S.V., Pickens, A.H., Parente, L.L.,
836 Ferreira, L.G., Song, X.-P., Hernandez-Serna, A., & Kommareddy, I. (2021). Rapid expansion of
837 human impact on natural land in South America since 1985. *Science Advances*, 7, eabg1620
- 838 Zalles, V., Hansen, M.C., Potapov, P.V., Stehman, S.V., Tyukavina, A., Pickens, A., Song, X.-P., Adusei,
839 B., Okpa, C., Aguilar, R., John, N., & Chavez, S. (2019). Near doubling of Brazil’s intensive row
840 crop area since 2000. *Proceedings of the National Academy of Sciences, USA*, 116, 428-435
- 841
- 842